Spring 1-1-2015

Monte Carlo Simulations of Polarized Light Propagating Through Optically Dense Media with Applications for Lidar Systems

Andrew Washington Gisler
University of Colorado at Boulder, andrew.gisler@gmail.com

Recommended Citation

Gisler, Andrew Washington, "Monte Carlo Simulations of Polarized Light Propagating Through Optically Dense Media with Applications for Lidar Systems" (2015). *Aerospace Engineering Sciences Graduate Theses & Dissertations*. 102.
https://scholar.colorado.edu/asen_gradetds/102

Monte Carlo Simulations of Polarized Light Propagating Through Optically Dense Media with Applications for Lidar Systems

by

Andrew W. Gisler

B.S. Physics, Yale University, 2008

M.S. Physics, University of Colorado, 2013

A thesis submitted to the
Faculty of the Graduate School of the
University of Colorado in partial fulfillment
of the requirements for the degree of
Master of Science
Department of Aerospace Engineering
2015

This thesis entitled:
Monte Carlo Simulations of Polarized Light Propagating Through Optically Dense Media with Applications for Lidar Systems
written by Andrew W. Gisler
has been approved for the Department of Aerospace Engineering

Jeffrey P. Thayer

Prof. Peter Pilewskie

Prof. Kristine Larson

Date ____________

The final copy of this thesis has been examined by the signatories, and we find that both the content and the form meet acceptable presentation standards of scholarly work in the above mentioned discipline.

Gisler, Andrew W. (M.S., Aerospace Engineering)

Monte Carlo Simulations of Polarized Light Propagating Through Optically Dense Media with Applications for Lidar Systems

Thesis directed by Prof Jeffrey P. Thayer

Active remote sensing systems, such as lidar, allow for distant measurements of various media and objects. Lidar systems are in use around the world to measure a variety of atmospheric parameters but retrieval primarily relies on a single-scattering assumption which breaks down in optically dense media such as clouds or turbid water. In a multiple-scattering regime, light that is scattered many times carries information about the incident light and the scattering medium and lidar systems are designed to take advantage of the information contained in the returned signal.

Experimental techniques and theoretical investigations need to go hand-in-hand to further understand of how lidar systems probe complex environments. In this thesis I develop a Monte Carlo simulation to track how the polarization of light is affected by scattering in an optically dense media and run simulations to illustrate how lidar measurements extract cloud microphysical properties.

Dedication

To everyone who took the time to listen.

Acknowledgements

I would like to thank my advisor Dr. Jeffrey Thayer for allowing me to tackle problems in my own way while always offering valuable advice and necessary grounding. My other two committee members have helped me immensely: Dr. Kristine Larson provided guidance on entering Aerospace Engineering and Dr. Peter Pilewskie taught me how to write Monte Carlo codes.

Many fellow Aerospace graduate students helped me along the way. In particular, Robert Stillwell showed me how to operate the INPHAMIS lidar system and Rory Barton-Grimley forced me to learn it even better.

There are many people at JILA who helped me in my previous life as a physicist. I would not be where I am today without the help and wisdom of Dr. David Nesbitt and the people I met in his group.

I have made many friends in Colorado and beyond who have helped me immensely outside the classroom and laboratory. Chief among them are the Rocky Mountain Runners, the Tally-Hos, and the residents of the Merwin plus.

I would like to recognize the financial support provided by ASTRA, LLC to enable this research. Dr. Geoff Crowley and Mr. Gerald Thompson were unselfish with their time, engaged with the topic, and interested in my success.

Finally, thanks to Mia for always always being there for me.

Contents

Chapter

Figures

Figure

Chapter 1

Introduction

Active remote sensing provides a powerful tool that we use to interrogate and learn about objects both near and far. In a lidar (light detection and ranging) system we transmit a pulse of light which scatters from an object, such as air molecules, aerosol droplets or terrestrial objects like buildings or trees, among other things. Some of the scattered light is collected on a detector and analyzed to determine the properties of the scattering medium. By recording the time between the transmitted and received signals, Δt, and knowing both the speed of light, c, and the index of refraction of the transmitting medium, n, the range to the scattering object can be calculated as $\Delta R = \frac{c\Delta t}{2n}$. The combination of range and recorded intensity alone can provide valuable information although many modern lidar systems also modify the wavelength and polarization of the light to learn about the identity and velocity of specific scatterers.

Turbid media is one in which the distribution of particles in the media reach sufficient optical density to scatter photons multiple times along the light path, consequently attenuating the light and making the light traverse paths substantially longer than if only scattered once. Most lidar systems work under a single-scattering assumption, that is,transmitted light scatters only once before returning to a co-aligned receiver. In many situations this is an appropriate assumption to make but in optically dense media, such as turbid water or clouds, it is impossible to ignore the contribution of multiple scattering. Three of the important considerations that multiple scattering introduces is an increase in the angular spread of returned photons (light will scatter away from its initial direction axis and back to the detector), stretching the return in time (light bounces back and forth in the cloud before returning to the receiver), and an increases the amount of depolarization in the returned light (light transmitted with one polarization will return with a different polarization).

For high particulate concentrations, extinction and multiple scattering will complicate the relation of observed backscatter to particulate concentration distributions. Lidar provides a means to derive quantitative information on particulate cloud distributions and optical properties over remote distances. By using a lidar technique known as INtrapulse PHAse Modification Induced by Scattering (INPHAMIS) [2], we have developed an invasive technique to determine the optical extinction through turbid water. The technique allows for the detection of sequential surfaces provided that the surfaces have different polarization properties. The signals of light scattering from each surface can then be separated based on differences in received polarization. The ambiguity in deconvolving the signal from two targets on one channel is then removed; the problem becomes two one-channel range finding problems.

The first application of this technique has been for shallow water depth measurement where the top surface of the water is polarization-preserving and the bottom surface is depolarizing. Typical bathymetric lidar systems utilize one green laser to detect both the top and bottom surfaces which becomes difficult when the water is very shallow (< 2 m). In this regime the signals from the two surfaces are overlapped in time. In the INPHAMIS technique, the top surface is detected in a polarization channel that is aligned with the incident laser polarization while the bottom surface is detected in a cross-polarized channel. This allows for very accurate depth measurements for waters ranging from 1 cm to many meters in depth, a depth range previously inaccessible by both lidar and sonar. By introducing a scattering surface into the water, the water depth to the target and the extinction of laser light through the water to the target and back can be used to determine the water turbidity. This is what we call an invasive technique in that it requires a target come in contact with the water.

However, the INPHAMIS technique is not limited to detection of hard surfaces as described above. Multiple scattering by suspended particles can introduce phase modification in the form of depolarization that would allow for differential detection of single- and multiple- scattered photons from optically dense media. Thus, a non-invasive, lidar remote-sensing technique for determining water turbidity could be developed.

In this thesis, the basis for a noninvasive remote sensing lidar technique for determining optical turbidity is then explored theoretically by exploiting the polarization attributes of multiple scattering in turbid media. The premise is that, by quantifying through lidar measurements the amount of depolarization attributed to the degree of multiple scattering, an estimate of the optical depth of the media from remote distance can be provided. By combining the invasive and noninvasive approach using the same lidar technology, a validation procedure can be developed to relate the remote observation of multiple scattering with the invasive measurement of optical depth.

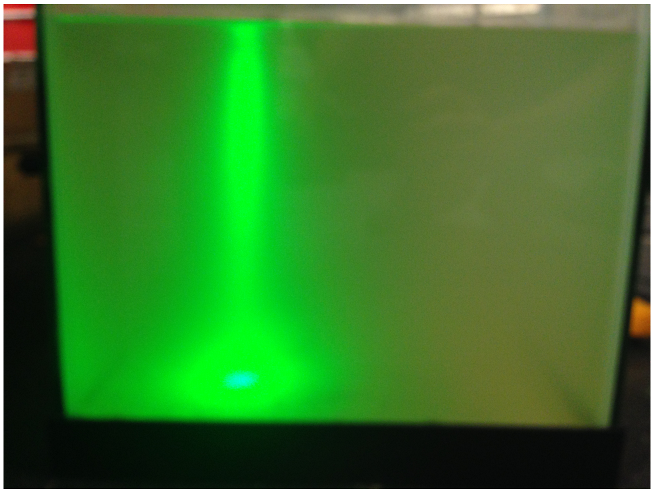

Figure 1.1: A picture of a 532 nm laser interacting with turbid water in an aquarium. The apparent spread of the reflected laser light is due to multiple scattering.

A demonstration of the invasive lidar technique for measuring extinction through turbid media is shown in Figure 1.2. Here, the INPHAMIS lidar system operating at 532 nm was positioned over a tank of turbid water. The INPHAMIS technique can provide centimeter range resolution to targets submerged underwater allowing for the position of a scattering target below the surface to be easily determined. A scattering target was then progressively lowered into the tank of turbid water and the intensity of the backscattered laser light off the target was recorded at incremental range steps. As the scattering target was lowered deeper into the water, the returned signal decreased due to the turbidity level of the water. Using a narrow field-of-view and observing the change in intensity with range, a two-way extinction measurement of $k = 0.25$ cm^{-1} was calculated by fitting the measurements to an exponential function (e^{-kx}). This is much larger than the absorption coefficient of water for the 532 nm laser light (~ 0.001 cm^{-1}) indicating that the extinction observed is largely due to the scattering of light from the suspended fine-grain sand present in the water. This measurement provides a direct means of determining the level of turbidity of the water and can be used as important information in determining the multiple scattering attributes of optically dense media.

Upon interacting with the turbid media, some of the multiply-scattered light will make it back to the detector to contribute to the measured signal and so understanding how this affects the amount of returned light will assist in the interpretation of extinction curves and measured extinction coefficients shown in Figure 1.2. For example, if the scattered light is predominately forward-scattered as opposed to side-scattered then the measured extinction coefficient may not have a simple transformation to particle density or size.

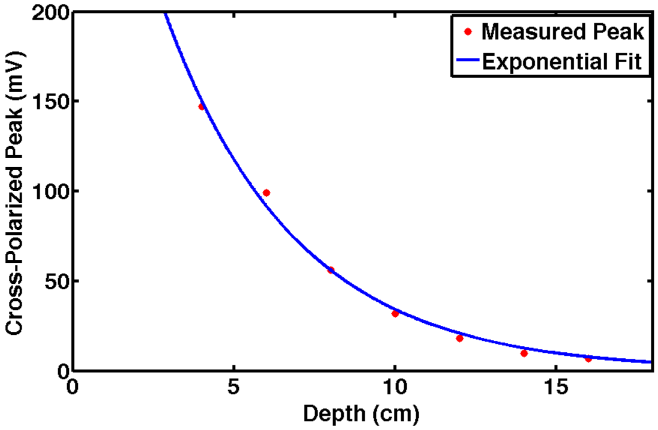

Figure 1.2: An extinction measurement performed by directing a lidar system at a scattering target which is progressively immersed at various depths in a tank full of turbid water. The fitted two-way extinction coefficient is 0.25 cm^{-1}.

The above influence of multiple scattering is widely known and our approach makes a novel contribution by making a measurement of the depolarization as a function of range and as a function of telescope field-of-view to retrieve estimates of optical density. Another technique that is commonly used to study multiple scattering is to look at the angular spread of light that arises from multiple scattering. This is typically done using two CCD cameras that receive different polarizations of light. By comparing these angular patterns with patterns produced by known particle distributions, people can learn about how the multiple scattering is both inducing depolarization and contributing to the angular spread of light.

These two multiple-scattering techniques have some important limitations. The first, whereby depolarization is recorded as a function of distance and field-of-view, misses out on the nuances present in the received patterns. The second technique, where images are recorded on CCD cameras, carries no range information. Our aim is to understand how a technique that can capture both pieces of the spatial pattern and range information can be useful to determining the properties of the optically dense media we are interrogating.

1.1 Multiple Scattering in Lidar

The single-scattering elastic backscatter lidar equation can be written in a form (from [3])

$$P(z) = \frac{K(z)}{z^2}\beta(z)e^{-2\gamma(z)} \tag{1.1}$$

where $P(z)$ is the received power from range z, $K(z)$ is the instrument and overlap function, $\beta(z)$ is the backscattering coefficient, $\gamma(z) = \int_0^z \alpha(z)dz$ is the optical depth at range z and $\alpha(z)$ is the extinction coefficient. Lidar systems exploit this equation and attempt to extract $\beta(z)$ and $\alpha(z)$ which often involves some assumption about the relation between the two. In order for this equation to remain valid, photons which are not exactly backscattered are assumed to be lost forever. Once the field-of-view (FOV) is large enough that multiply scattered photons may remain in the field-of-view and their contribution can be captured, then this equation must be modified in some way.

The first lidar experiments that dealt with multiple scattering was work by Milton, Anderson, and Browell in which they observed laser light reflecting from clouds [4]. The received signal was 2-3 times that predicted by a single-scattering lidar equation of the form of Equation (1.1). They attributed this to multiply scattered light entering the receiver which was eventually confirmed by laboratory experiments by Pal, Ryan, and Carswell [5]. From there, many groups have worked on how to extract relevant physical information on clouds based on multiple scattering returns. Further lidar multiple scattering studies are presented in Chapter 3 and in the book chapter by Bissonnette [3].

Backscattered light has also proven useful for analyzing biological cell suspensions. There are many cases where a remote measurement of biological tissue *in vivo* is advantageous to *in vitro* methods. For many biological cases in which the sample is close to the transmitter and receiver, there is an opportunity to measure a wide range of angles which allows for a wealth of information that is usually unavailable to the lidar community where observed light is nearly perfectly backscattered. This has led to a great deal of development in Monte Carlo codes as well as experimental techniques to learn about the reflectance of cell cultures.

Though multiple scattering is a field with a great history of development, increased computer speed and advanced detector technologies are now allowing for more and more information to be predicted and observed. This thesis aims to study multiple scattering from the ground up, as a sort of manual for understanding its effects. Additionally, a Monte Carlo code has been written which can be used in conjunction with proposed experimental techniques in order to evaluate and analyze multiply scattered returns from media such as clouds and turbid water.

Through the use of a self-developed Monte Carlo code, we are investigating a) how the angular spread of returned photons depends on recorded range, b) what new information this can provide about the particles doing the multiple scattering, and c) whether this can be incorporated into a lidar transmitter/receiver using current technologies. This Monte Carlo code has wide implications for polarization-sensitive lidar systems, such as the INPHAMIS technique. Through analysis of the theoretical backscatter returns we plan to design experiments to remotely characterize optically dense media. Although beyond the scope of this thesis, experimental verification could include multiple-field-of-view measurements with an INPHAMIS system as well as utilizing CCD cameras to image the angular distribution of the returned light.

There are two main results that have come out of these simulations for application to wide-field-of-view lidar systems. The first is that we can calculate the optical depth of a cloud or of turbid media by measuring the depolarization of the returned lidar pulse, as long as the field-of-view of the receiver is large enough to observe multiple scattering. As the laser pulse penetrates the cloud it is depolarized by multiple scattering. The number of scattering events is related to the total optical depth (or the optical depth at a given range) so we can then relate the amount of depolarization to the optical depth of the medium. The second result is that the observed angular spread of the returned multiply-scattered light is related to the size of the particles. In Mie theory, as the particle size increases, the angular width of the forward scattering peak decreases, and therefore we see that the angular spread of the returned light is also smaller. By taking measurements with different field-of-view we can then work out how the lidar pulse is spreading laterally through the medium, which then informs on the particle size. These two measurements, taken simultaneously, can serve to identify two important cloud parameters.

Chapter 2

Monte Carlo

Monte Carlo programs were devised in 1949 by Metropolis and Ulam in order to solve problems which could neither be solved analytically (few particles) or statistically (ensembles of particles) [6]. The method involves sampling single chains of stochastically determined events. In radiative transfer problems, each chain can be thought of as the trajectory of a single photon where at each step known distributions for path length, absorption probability, and scattering angle are sampled to determine how the photon propagates through a medium. By running through a large number of photon trajectories, the shot noise can be reduced to an acceptable level.

A Monte Carlo program has an advantage over many other types of radiative transfer simulations because it requires very few simplifying assumptions or approximations. This allows for calculations involving complex media (varying densities or particle identities) and complex geometries (lidar arrangement or cloud shape). Another advantage is that the problem can be broken up and analyzed at each step so contributions from single, double, and higher-order scattering orders can be separated. Added flexibility comes at the price of computation time and resources, although as computers increase in speed it is becoming more feasible to perform complex calculations.

2.1 Development

Monte Carlo programs for use in modeling of light interactions with clouds was pioneered by Plass and Kattawar [7, 8, 9, 10, 11, 12]. For the lidar geometry, in which the detector is small and far from the scattering medium, so few photons return to the detector that Monte Carlo codes become increasingly inefficient. This is exacerbated by the fact that for particles comparable to and larger than the wavelength of interrogating light, most of the scattering is in the forward direction, away from the lidar receiver. The solution to this problem is to lower the variance by introducing analytic computation into the stochastic Monte Carlo code.

Many different solutions have been implemented to reduce the large variance inherent to processes with small count rates, such as Monte Carlo codes for Lidar returns. Plass and Kattawar forced photons to scatter in favorable directions and assigned a weight to each photon to track the probability of a given trajectory [9]. A far more powerful technique known as statistical estimation was developed by Plass and Kattawar [12] and refined by Kunkel and Weinman[13] and Poole, Venable, and Campbell [14, 15]. This is the chief variance reduction method employed in this thesis. At each collision point, an analytical probability that the photon returns directly to the lidar receiver is used to increase the number of observations. This probability depends on the probability to scatter in the correct direction, the probability to travel without further interaction to the lidar receiver, the receiver aperture, and the distance to the receiver. At the end of the Monte Carlo simulation, the sum of all of these probabilities for all collisions is used as the returned signal rather than a count of the total number of photons which do make it into the lidar receiver. Another variance reduction strategy is to artificially increase the number of backward-direction photon scattering events and assigning a weight to these trajectories to correct for this non-physical increase [16]. Monte Carlo codes have a drawback in that the results are specific to a given optical depth. One way around this is to create scaling laws that relate optical depth to total number of scattering events, run a calculation for a very deep optical depth, then sum results for different scattering orders with appropriate weighting for the optical depth of interest[17]. There are also methods that exploit rotational symmetry in the multiple scattering geometry that allow for the calculation at a single radial point on a detector to contribute azimuthally around a detector[18]. The choice of any of these variance reduction techniques can reduce computation time by factors of 2 to 10 dependent on the specifics of the problem.

2.2 Stokes Vector Monte Carlo

A Monte Carlo program works by taking one photon at a time and propagating it through a medium based on random sampling of probability distributions. The method laid out below is based on work by Bartel and Hielsher [19] and is presented in detail by Ramella-Roman, Prahl, and Jacques [20]. At each scattering event, reference planes are rotated utilizing Euler angles (method 2 in [20]) to track the polarization of the particle through the medium. For this simulation, each photon will begin at an initial position $\vec{r}_0$ with an initial direction vector $\hat{u}_0$ and an accompanying vector that defines the electric field reference plane $\hat{v}_0$. The initial Stokes vector

$$\vec{S} = \begin{bmatrix} I \\ Q \\ U \\ V \end{bmatrix} = \begin{bmatrix} E_x^2 + E_y^2 \\ E_x^2 - E_y^2 \\ E_a^2 - E_b^2 \\ E_l^2 - E_r^2 \end{bmatrix} \tag{2.1}$$

where the subscripts refer to basis sets with standard cartesian vectors $(\hat{x}, \hat{y})$, cartesian vectors rotated by 45° $(\hat{a}, \hat{b})$, and a circular basis $(\hat{l}, \hat{r})$. Note that the reference vector $\hat{v}$ defines the $\hat{x}$ polarization direction. The scattering medium is set up as infinite in the $\hat{x}$ and $\hat{y}$ directions and extends from $z = 0$ to $z = \bar{\tau}$. In the negative half-space $z < 0$ there are no interactions which, although unrealistic, allows for us to study solely the effects of the cloud.

Each photon is then propagated a distance τ through the scattering medium which is sampled according to a probability $P(\tau) = e^{-kz}$ where k is an extinction coefficient. A random ξ is sampled uniformly on the open interval $(0, 1)$ then the distance is calculated as $\tau = -\ln(1 - \xi)/k$. A comparison of 10^8 simulated lengths along with the expected distribution are shown in Figure 2.1. The position of the particle is updated to $\vec{r} = \vec{r}_0 + \tau\hat{u}$ and a scattering event takes place.

In each scattering event, a scattering angle θ and rotation angle of the scattering plane ϕ must be chosen. The phase function that defines the probability with which these are sampled, $P(\theta, \phi)$, depends both on the incident Stokes vector $\vec{S} = [I_0, Q_0, U_0, V_0]$ and the scattering matrix

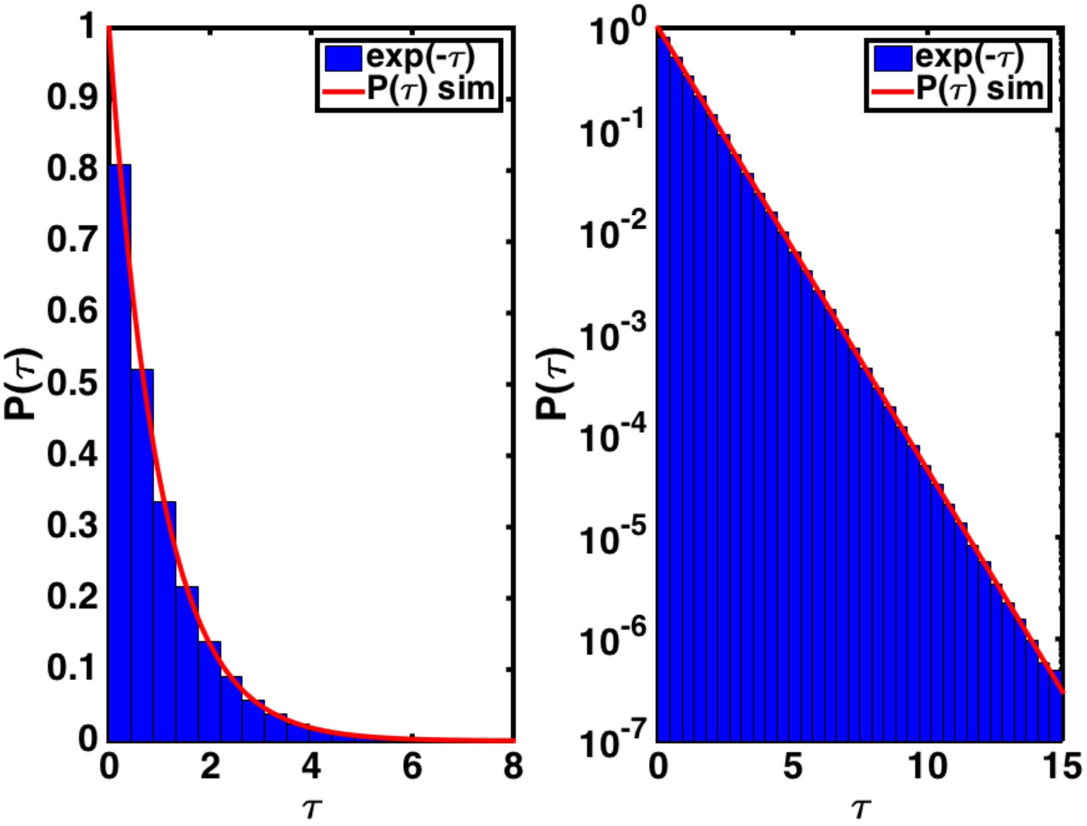

Figure 2.1: Probability distribution for the propagation distance in both a linear (left) and log (right) plot for 10^8 total trajectories with k=1.

$M(\theta)$

$$P(\theta,\phi) = M_{11}(\theta)I_0 + M_{12}(\theta)\left[Q_0\cos 2\phi + U_0 \sin 2\phi\right] \tag{2.2}$$

The scattering matrix can be written for spherical particles as

$$M(\theta) = \begin{bmatrix} M_{11}(\theta) & M_{12}(\theta) & 0 & 0 \\ M_{12}(\theta) & M_{11}(\theta) & 0 & 0 \\ 0 & 0 & M_{33}(\theta) & M_{34}(\theta) \\ 0 & 0 & -M_{34}(\theta) & M_{33}(\theta) \end{bmatrix} \tag{2.3}$$

Where the matrix elements are calculated using Mie theory [21] based on an algorithm by Prahl and Mätzler [22].

$$\begin{aligned} M_{11}(\theta) &= \frac{1}{2}\left(|S_2(\theta)|^2 + |S_1(\theta)|^2\right) \\ M_{12}(\theta) &= \frac{1}{2}\left(|S_2(\theta)|^2 - |S_1(\theta)|^2\right) \\ M_{33}(\theta) &= \frac{1}{2}\left(S_2^*(\theta)S_1(\theta) + S_2(\theta)S_1^*(\theta)\right) \\ M_{34}(\theta) &= \frac{i}{2}\left(S_2^*(\theta)S_1(\theta) - S_2(\theta)S_1^*(\theta)\right) \end{aligned} \tag{2.4}$$

Where S_1 and S_2 are functions of the size parameter $x = \frac{2\pi r}{\lambda}$, the complex index of refraction of the particle n, and summations of spherical Bessel functions, spherical Henkel functions, and Ricatti-Bessel functions. A complete description is provided in [21].

If the particle size is much less than the wavelength ($x \ll 1$), Mie scattering approaches a Rayleigh scattering limit in which the scattering matrix looks like

$$M_{\text{rayleigh}}(\theta) = \frac{1}{2}\begin{bmatrix} \cos^2\theta + 1 & \cos^2\theta - 1 & 0 & 0 \\ \cos^2\theta - 1 & \cos^2\theta + 1 & 0 & 0 \\ 0 & 0 & 2\cos\theta & 0 \\ 0 & 0 & 0 & 2\cos\theta \end{bmatrix} \tag{2.5}$$

For incident linear polarized light $\vec{S} = [1,1,0,0]$ the phase function becomes

$$P_{\text{rayleigh}}(\theta,\phi) = \frac{1}{2}(1 - \sin^2\theta\cos^2\phi) \tag{2.6}$$

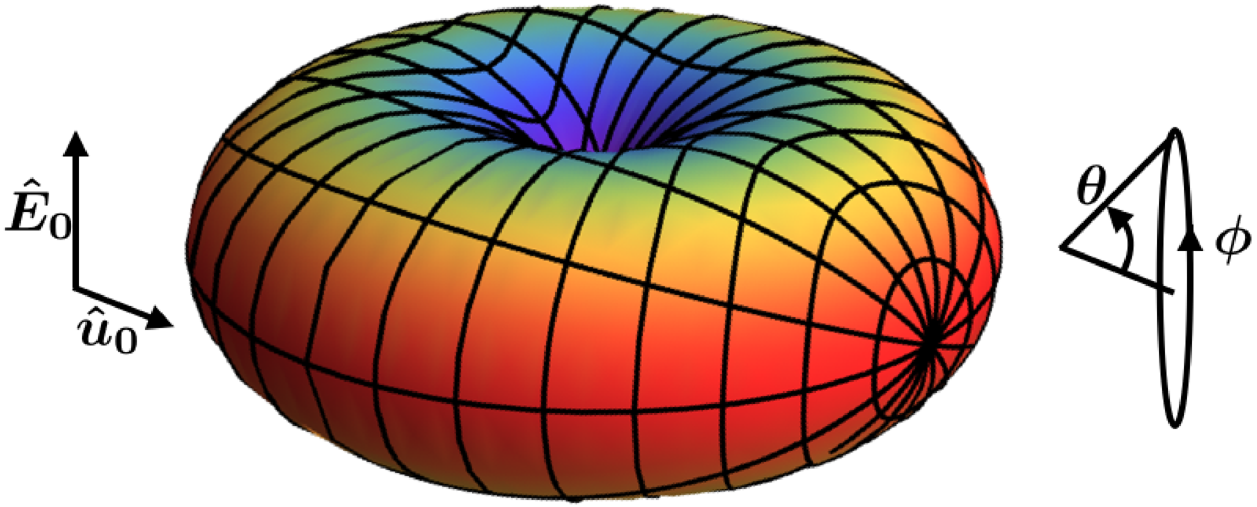

Figure 2.2: Probability distribution of the scattering direction for linearly polarized light incident on a particle whose radius is much less than the wavelength of light (Rayleigh scattering). The scattering angle θ is calculated with respect to the propagation direction $\hat{u}$ and ϕ is the azimuthal angle with respect to the incident polarization angle $\hat{E}$

This particular phase function is shown in Figure 2.2.

To perform the sampling of this bivariate phase function $P(\theta,\phi)d\Omega$, a rejection method is used. First three random numbers are sampled uniformly on their open intervals, $\alpha \in (0,\pi)$, $\beta \in (0,2\pi)$, $\delta \in (0,P(0,0)))$. If $\delta < P(\alpha,\beta)d\Omega$, then $\theta = \alpha$ and $\phi = \beta$, otherwise the three values α, β, δ are resampled.

Utilizing the scattering angles, the reference vectors $\hat{u}$ and $\hat{v}$ must be rotated into the new plane through the use of Euler angles. To rotate a vector $\vec{p}$ around a unit vector $\hat{k}$ by an angle σ the vector $\vec{p}$ is multiplied by the by the Euler matrix

$$R_{\text{euler}}(\hat{k},\sigma) = \begin{bmatrix} k_x k_x v + c & k_y k_x v - k_z s & k_z k_x v + k_y s \\ k_x k_y v + k_z s & k_y k_y v + c & k_y k_z v - k_x s \\ k_x k_z v - k_y s & k_y k_z v + k_x s & k_z k_z v + c \end{bmatrix} \tag{2.7}$$

where $\hat{k} = [k_x, k_y, k_z]$ and $c = \cos\sigma$, $s = \sin\sigma$, $v = 1 - \cos\sigma$. Two rotations must be performed, one on each of our reference vectors $\hat{v}$ and $\hat{u}$. First, $\hat{v}_{\text{new}} = R_{\text{euler}}(\hat{u},\phi)\hat{v}$ then $\hat{u}_{\text{new}} = R_{\text{euler}}(\hat{v}_{\text{new}},\theta)\hat{u}$.

Next, the Stokes vector is rotated and acted upon by the scattering matrix $M(\theta)$. To rotate a Stokes vector through an angle β a rotation matrix of the form

$$R(\beta) = \begin{bmatrix} 1 & 0 & 0 & 0 \\ 0 & \cos 2\beta & \sin 2\beta & 0 \\ 0 & -\sin 2\beta & \cos 2\beta & 0 \\ 0 & 0 & 0 & 1 \end{bmatrix} \tag{2.8}$$

is used. The new Stokes vector is then

$$\vec{S}_{\text{new}} = M(\theta)R(\phi)\vec{S} \tag{2.9}$$

To maintain equal weight for each photon throughout the scattering process, the Stokes vector after a collision is normalized by the first value $\vec{S} = \vec{S}/\vec{S}(1)$. The process then begins anew with the selection of a new τ.

Once the photon reaches the boundaries the process ends and a new photon trajectory is launched from the beginning.

The above method works well for tracking how a laser pulse interacts with a cloud, but for a lidar system where the angular size of the detector as viewed from the cloud is very small it is quite inefficient. As discussed in Section 2.1 there are many methods to increase the computational efficiency of a Monte Carlo radiative transfer scheme especially with regards to the specifics of the lidar geometry.

To increase the efficiency of the calculation, at each scattering event a probability to directly scatter back to the lidar detector is calculated. This is related both to the phase function to scatter through an appropriate angle as well as the probability travel through the entire cloud without scattering.

$$p_{\text{back}} = \frac{P(\theta_{\text{back}}, \phi_{\text{back}})}{P(0,0)} e^{-k\tau_{\text{back}}} \tag{2.10}$$

The Stokes vector is rotated one last time to orient it into the detector reference frame. This detector sits in the x-y plane (perpendicular to the initial direction vector $\hat{u}$). The third reference direction is calculated from the two $\hat{w} = \hat{v}_{\text{back}} \times \hat{u}_{\text{back}}$ and from that an angle $\varepsilon = \tan^{-1}\left(\frac{-v_{\text{back},z}}{w_{\text{back},z}}\right)$ is calculated. Another angle $\psi = \tan^{-1}(\frac{u_{\text{back},y}}{u_{\text{back},x}})$ is also found. Finally the Stokes vector is rotated twice and modified by the probability to scatter to the detector

$$\vec{S}_{\text{final}} = p_{\text{back}} R(\psi) R(\varepsilon) \vec{S} \tag{2.11}$$

Once in the detector plane, the Stokes vector can be passed through any sort of polarizer/retarding plate combination in order to analyze any particular element of the Stokes vector.

Along with information about the Stokes vector, information on the total distance a photon travels is stored to facilitate the retrieval of range-resolved signal levels. Additionally, scattering events are tagged by their apparent position in the sky with respect to a detector which allows for a transformation into an x-y position on a detector image plane.

One beauty of Monte Carlo simulations is the flexibility in framing the problem, though this comes at the cost of computation time. It is relatively straightforward to implement complexities such as particle size distribution, variable density, multiple types of scatterers, finite cloud dimensions, etc. In the results that follow, many of these variables will be held constant in an effort to isolate and quantify the multiple scattering effect.

Chapter 3

Monte Carlo Results

The power of Monte Carlo simulations is the ability to replicate experimental conditions very closely. As shown below, the lidar observations are highly dependent on problem parameters such as distance to cloud, particle size distribution, particle density, particle index of refraction, particle shape, etc. The goal of the simulations presented here is not to describe what any individual experiment would observe, rather we would like to build up a picture of multiple scattering that can be used to understand observations of multiple scattering and to inform on how a lidar might be optimized to observe multiple scattering.

In order to quantitatively present the effects that multiple scattering has on lidar returns some experimental conditions must be chosen. For these simulations, a lidar transmitter/receiver sits 1 km from a cloud which has a depth of 100 m while being infinite in the transverse direction. The transmitting laser pulse has an infinitesimally small width and zero beam divergence, which is non-physical although these results will hold in the limit that the beam divergence is smaller than the detector FOV. The extinction coefficient of the cloud varies in different simulations from 10 to 30 km^{-1} (the total optical depth τ_{total} of the cloud varies from 1-3). The index of refraction of the particles will be that of water, $n = 1.33$ and there are two different particle sizes (0.075 μm and 0.85 μm). The transmitting laser has a wavelength of 633 nm (HeNe laser) so the two particle sizes correspond to a size parameter $x = \frac{2\pi r}{\lambda}$ of 0.74 and 8.43 respectively. These particles sizes correspond to haze droplets, not to cloud droplets, as will be discussed further in Chapter 4. Phase functions for these two particle sizes and for an incident linear polarization are shown in Figure

3.1. Note that for two simulations with the same τ_{total} and the different particle sizes, the particle density will be different due to differing scattering cross sections.

3.1 Effects of Multiple Scattering

Most Lidar systems operate in a single-scattering regime but in an optically dense media such as a cloud or turbid water, this assumption breaks down. For sufficiently narrow laser divergence and receiver field of view, it is still possible to observe primarily single scattered photons. In a Monte Carlo program it is possible to separate returned photons by scattering order, returned angle, and exact range. This permits analysis of different types of scattering trajectories.

The easiest scattering order to analyze is the first order. These photons are ones that undergo exactly 180° backscattering. For scattering from spherical particles with linear incident polarization, the returned light will have the exact same polarization as the transmitted light; spherical particles do not depolarize incident linear polarization [21]. Particles of different shapes and orientations will however depolarize perfectly backscattered light so depolarization is often used to differentiate water clouds from ice-crystal clouds [23, 24, 25]. Figure 3.2 shows the single-scattered return from two different haze-clouds of different optical depths (extinction coefficients). As the optical depth increases, more total light is reflected but this light is also concentrated near the detector, the high optical density attenuates the signal as photons are scattered away from their direct path. The total range of the single-scattered photons also stops directly at the cloud boundaries.

As the field-of-view of the receiver is opened up, the receiver becomes sensitive to multiply scattered photons. Figure 3.3 shows signals from multiple fields-of-view (labelled by the half-FOV) for the two different optical-depth mist-clouds. The smallest field of view for each (0.1 mrad) closely approximates the single-scattered light from Figure 3.2. As the field of view increases, more light is allowed in to the detector making the cloud appear brighter than a single-scattering assumption would predict [4, 5]. The cloud also appears to extend beyond its physical boundary due to photons rattling around inside the cloud, taking more time to return to the detector.

Once photons are multiply scattered some depolarization can occur, and the best way to

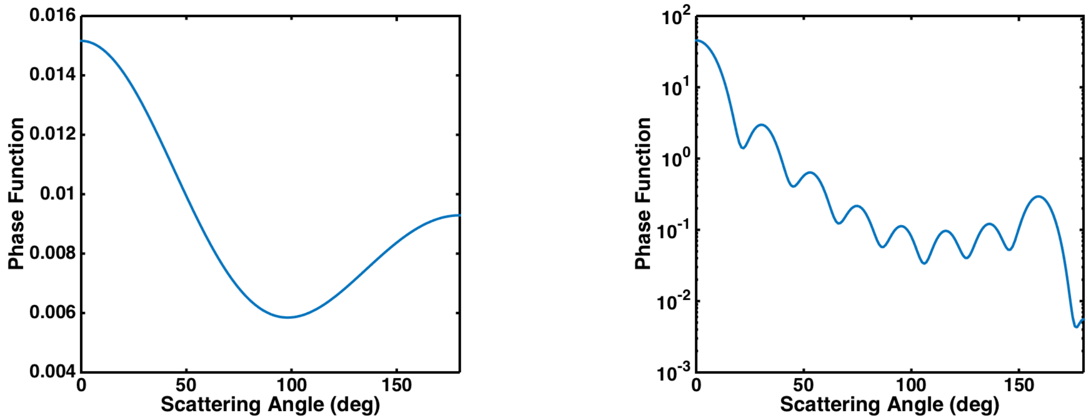

(a) Phase function for size parameter $x = 0.74$

(b) Phase function for size parameter $x = 8.43$

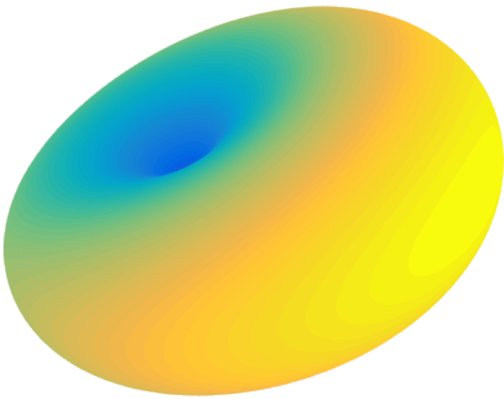

(c) Three dimensional Phpase function for size parameter $x = 0.74$

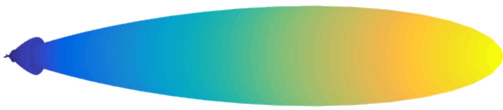

(d) Three dimensional phase function for size parameter $x = 8.43$

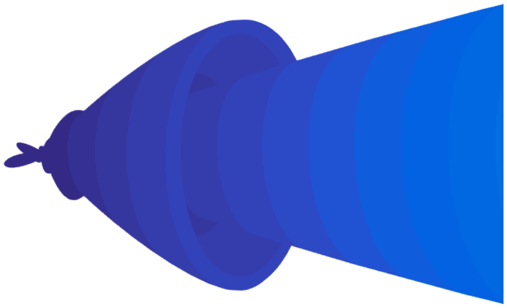

(e) Zoom in of the size parameter $x = 8.43$ three dimensional phase function shows backscatter lobes

Figure 3.1: Mie phase functions for incident linear polarization for small (a,c) and large (b,d,e) particles. For the three-dimensional phase functions (c,d,e), the initial direction is to the right and the initial polarization is vertical. The color (minimum of blue, maximum of yellow) indicates the magnitude of the phase function.

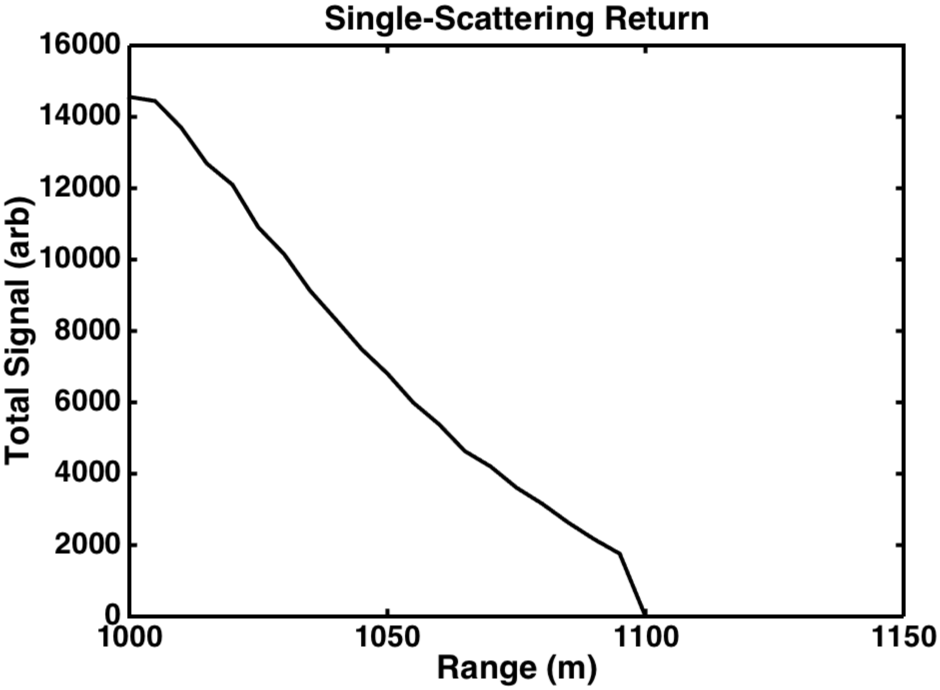

(a) $\tau_{\text{total}} = 1$

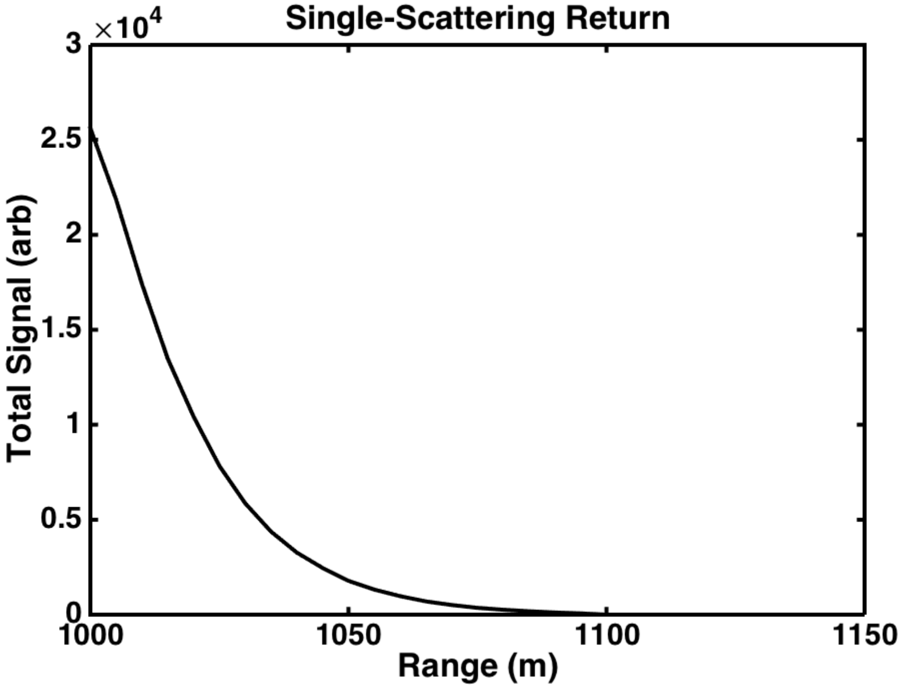

(b) $\tau_{\text{total}} = 3$

Figure 3.2: Single scattering backscatter return ($\theta_{\text{scat}} = 180°$) from clouds of size parameter $x = 0.74$ with two different total optical depths (a) $\tau_{\text{total}} = 1$ and (b) $\tau_{\text{total}} = 3$.

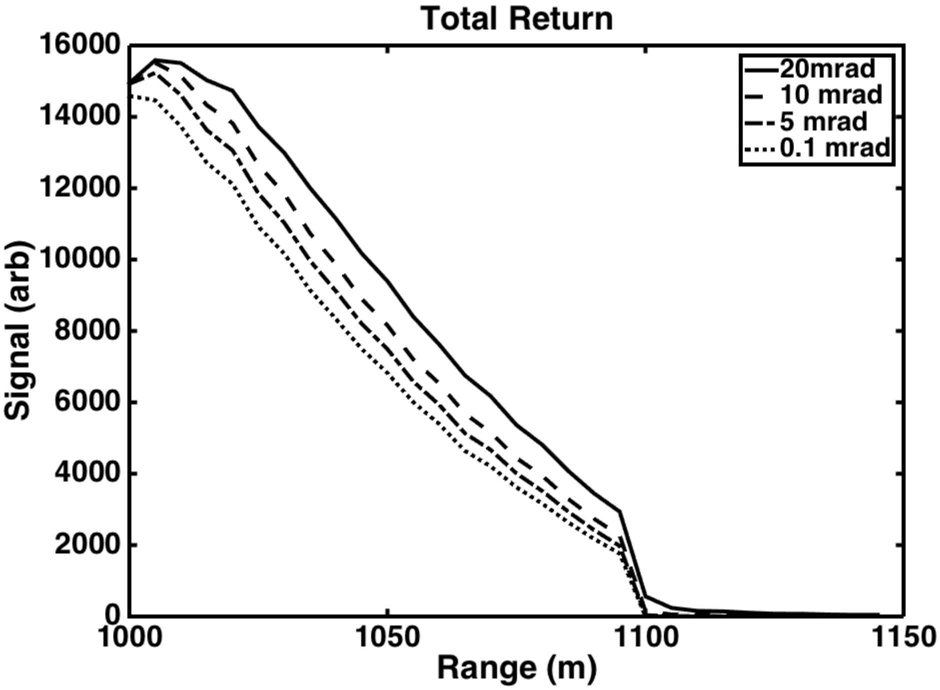

(a) Total returned signal for $\tau_{\text{total}} = 1$

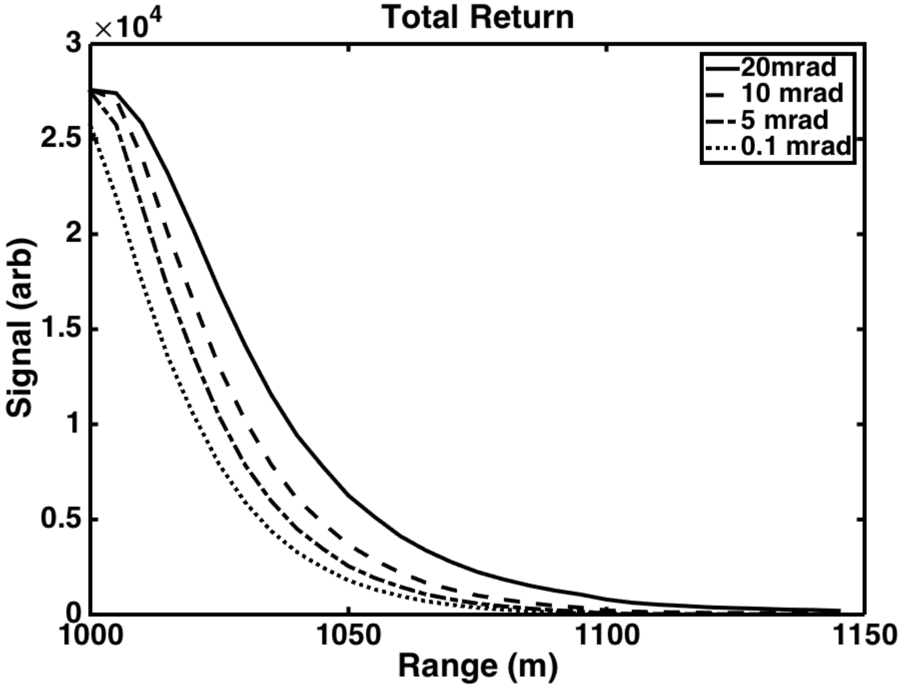

(b) Total returned signal for $\tau_{\text{total}} = 3$

Figure 3.3: Total backscatter signal from clouds with size parameter $x = 0.74$ size from a range of field-of-views and two different total optical depths.

view this is by opening the field-of-view. For a fixed wide field-of-view and spherical particles, separating returns which are co- and cross-polarized to the transmitted photons illustrate the change in depolarization due to multiple scattering. The co-polarized returns will include both single- and multiple-scattered photons while the cross-polarized signal will only come from multiple scattering. As a function of range this is shown for a half-FOV of 10 mrad for a single different total optical depth in Figure 3.4a. When more scattering occurs, as in the $\tau_{\text{total}} = 3$ case, more of the returned light is depolarized. In Figure 3.4b, the contribution to the total signal from each scattering order for the same FOV is plotted. The single-scattering events are dominant throughout the range in this case but the higher order terms become increasingly important at larger ranges. This is very dependent on the total field of view and total optical depth, as Figure 3.3 suggests. Many other studies have investigated the relative ratios of different scattering orders as a function of range [26, 13, 16, 27, 28, 17, 29, 30]. Using Monte Carlo simulations is a good way to determine how important multiple scattering would be for a given lidar geometry.

Before progressing with the quantitative analysis, it is also possible to combine much of the data already referenced into a single contour plot of the signal as a function both of range and of received angle as in Figure 3.5. When plotted in this way the single-scattered co-polarized return stands out at a viewing angle of 0°. The off-axis co-polarized signal (c and d) shows the strength of the second- and higher-order scattering that reaches a maximum part way into the cloud. The cross-polarized signal (e and f) also peaks part-way through the cloud but does so at a somewhat high return angle that depends on the extinction coefficient. For a higher extinction coefficient (higher τ_{total}) this peak occurs at a lower range and a lower return angle because the mean free path of photons through the cloud is shorter. This hints at an idea that will be developed in section 3.2, multiple fields-of-view are necessary in order to work out properties of the cloud and the choice of these fields-of-view will depend on cloud properties such as droplet size and optical density as well as geometrical considerations.

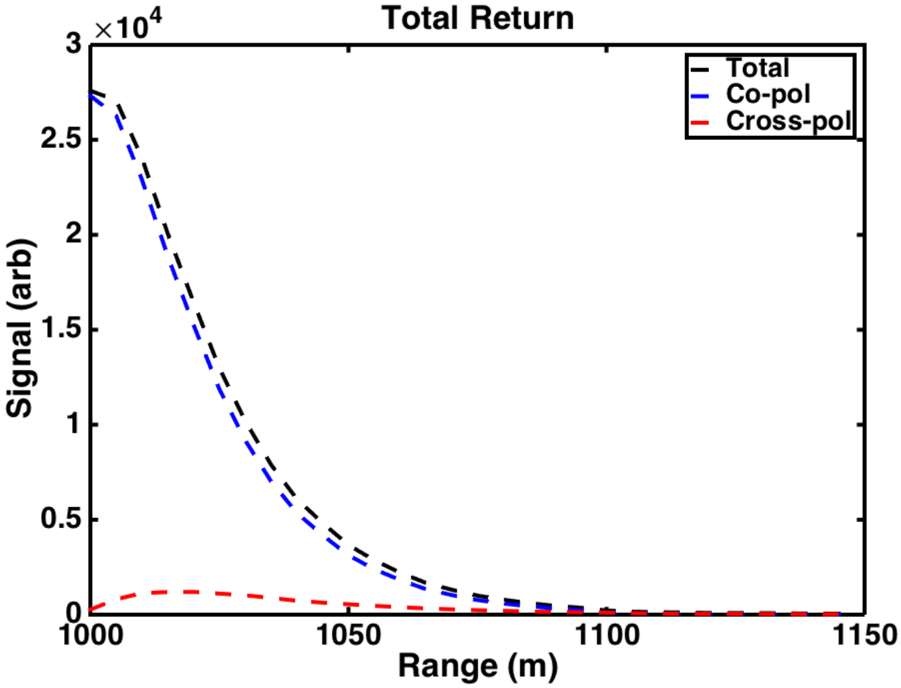

(a) Polarization dependent return for $\tau_{\text{total}} = 3$

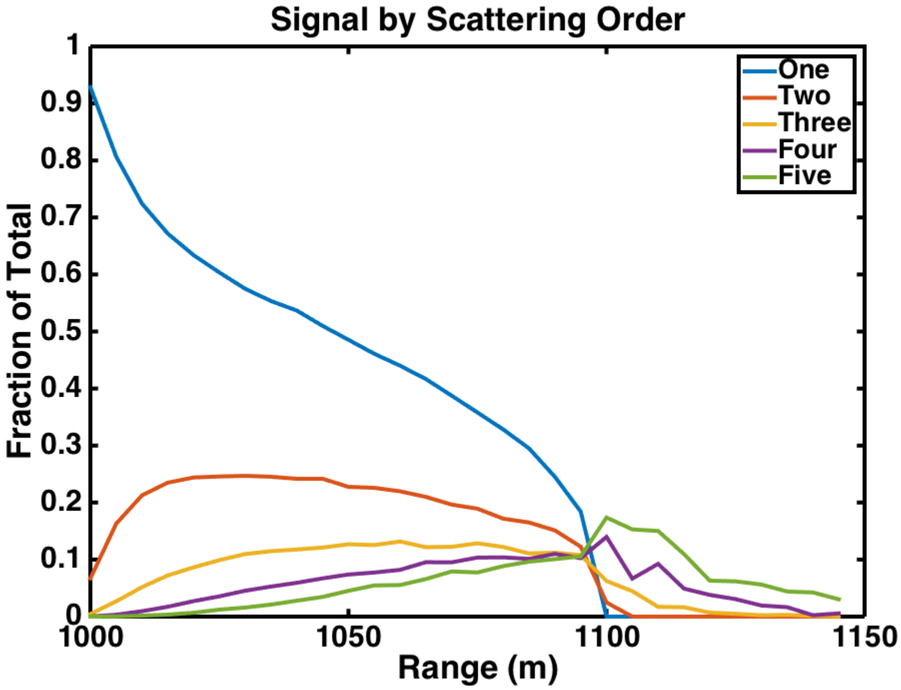

(b) Contribution from different scattering orders$\tau_{\text{total}} = 3$

Figure 3.4: Two different plots of range-dependent received signal from clouds with size parameter $x = 0.74$ and a receiver half-field-of-view of 10 mrad. (a) Polarization-dependent return and (b) fractional return by scattering order

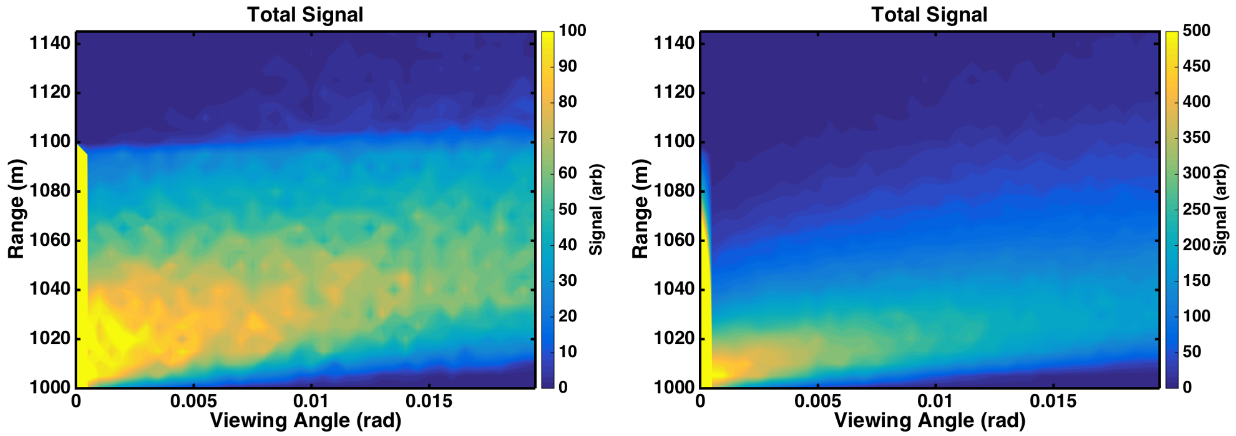

(a) $\tau_{\text{total}} = 1$ (b) $\tau_{\text{total}} = 3$

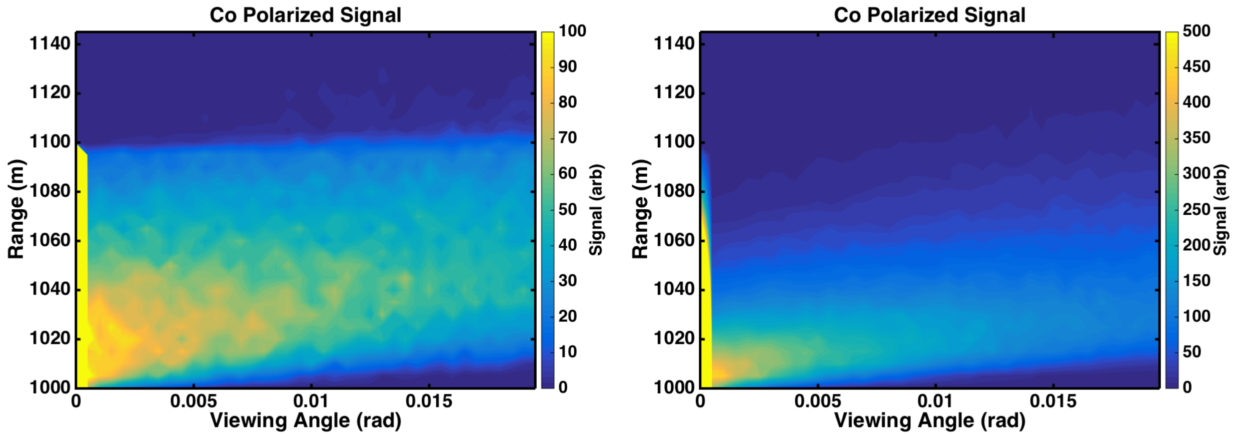

(c) $\tau_{\text{total}} = 1$ (d) $\tau_{\text{total}} = 3$

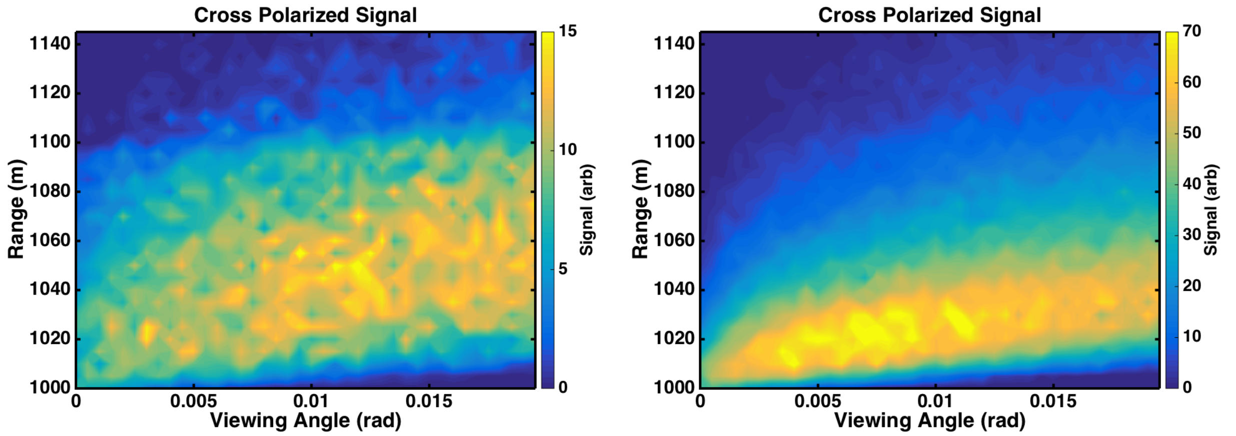

(e) $\tau_{\text{total}} = 1$ (f) $\tau_{\text{total}} = 3$

Figure 3.5: Contour plots of the returned signals from clouds with size parameter $x = 0.74$ with two different total optical depths. The signals are plotted against range and against viewing angle (or half-FOV).

3.2 Angular Spread

Multiple-field-of-view lidars are an established and powerful technique to analyze multiple scattering effects [31, 32, 33]. These systems have methods to quickly vary the field of view of the receiving telescope to capture signals as a function of range on a short enough timescale to not be confused by changes in cloud structure. One way that this works in practice is to use a rotating disk that has different sized-holes drilled at a constant radius as the field stop in a telescope. As the disk rotates, different sized holes lead to different fields of view and by timing the rotation of the disk to the firing of the laser it is possible to record very quickly signals for different FOVs [34].

The need for multiple field-of-views is to analyze how the lidar pulse spreads transverse to its initial direction. Shown in Figure 3.6 is the total signal observed below a given half FOV for both the co- and cross-polarized channels and for different particle sizes. The small particles have a strong single-scattered return at the smallest FOV and due to the wide shape of the phase function (Figure 3.1a) the cross-polarized signal comes back from a very high FOV angle. For the large particles, due to the low backscatter in the phase function (Figure 3.1b) the single scattered signal is a much lower percentage of the total signal. Also due to the very tight forward peak of the phase function much more cross-polarized signal comes from lower FOV than in the small particle case.

The way in which the laser pulse spreads through the cloud depends on the extinction coefficient and the particle size so the goal of a MFOV inversion scheme is to extract these two parameters. From these parameters other physical quantities of interest such as liquid water content (LWC) and broadband extinction can be derived. Bissonnette et. al. describe such a scheme and their lidar retrieval is able to extract droplet sizes and LWC within around 10% of measured data [35]. MFOV retrieval algorithms are typically designed from analytic or semi-analytic formulas for the multiple scattering contribution and then tested using Monte Carlo codes and controlled experiments. When designing a MFOV lidar system the choice of field-of-views is essential for gathering information. Veselovskii et. al. performed a study on the optimal number of FOVs in order to extract the most information with the least experimental complexity and found that 5-6

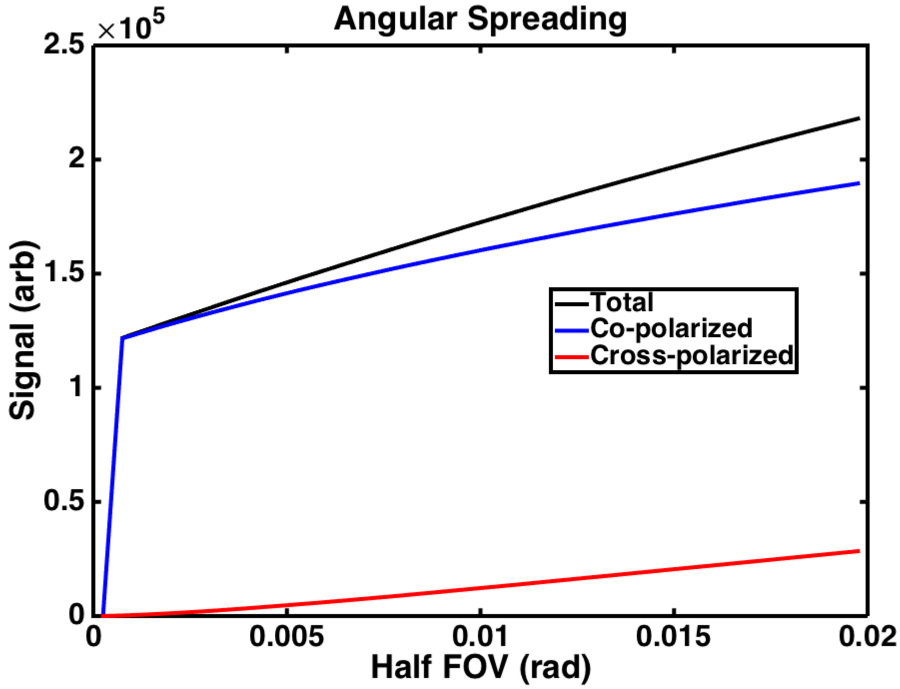

(a) Size parameter $x = 0.74$ $\tau_{\text{total}} = 3$

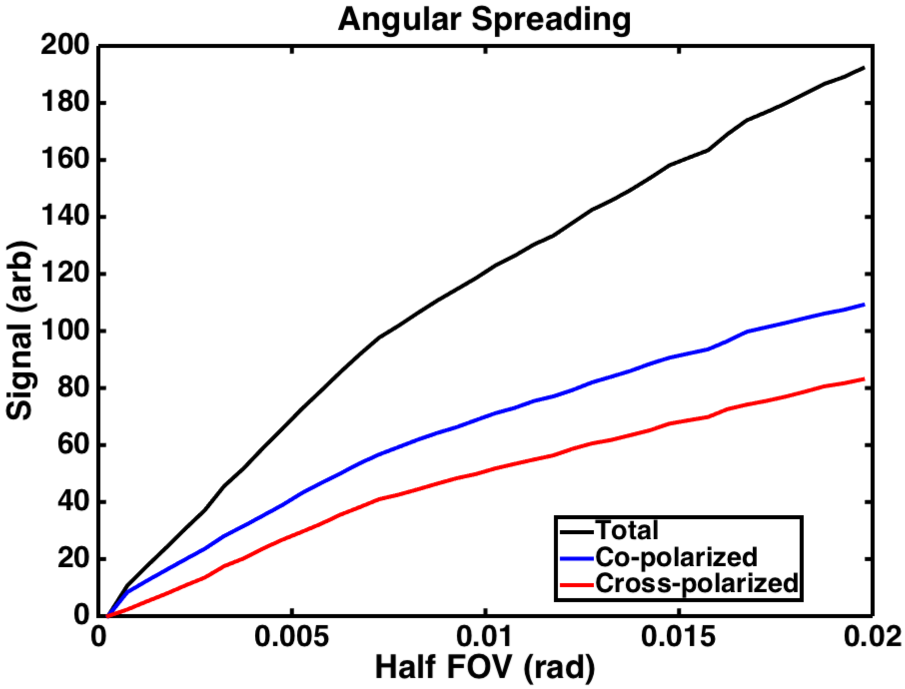

(b) Size parameter $x = 8.43$ $\tau_{\text{total}} = 3$

Figure 3.6: Signal versus half-field-of-view for clouds of different size particles and the same optical depth

FOVs are needed and that the magnitudes of the FOVs depends on the range to the cloud [36].

One weakness of Monte Carlo codes is that they do not inform on how to craft an inversion algorithm to extract physical quantities from observations. They do however serve as a testing ground for a given algorithm that is designed from analytic and semi-analytic multiple-scattering formulae.

3.3 Depolarization

The earliest method used to evaluate multiple scattering was to take a ratio of the returns from the cross- and co-polarized channels called the linear depolarization ratio [37]

$$\delta = \frac{I_\perp}{I_\parallel} \tag{3.1}$$

Very generally, the more multiple scattering the higher this ratio will be. As discussed in earlier sections, this ratio will be dependent on the experimental parameters such as FOV and particle size/density etc. Another metric which encapsulates similar information is the linear polarization contrast

$$\delta_{\mathrm{LPC}} = \frac{I_\parallel - I_\perp}{I_\parallel + I_\perp} \tag{3.2}$$

The linear polarization contrast is constrained to lie between -1 and 1 whereas the depolarization can take on any value greater than 0 (but is generally less than 1). As light travels through the cloud and scatters more than once, the depolarization will increase and the linear polarization contrast will decrease. For unpolarized light, or equal quantities of co- and cross-polarized signal, $\delta_{\mathrm{LPC}} = 0$. The effect that multiple scattering has on this quantity is shown in Figure 3.7a. The light returned in the smallest field of view maintains the initial linear polarization since this light is scattered only once before returning to the receiver. As the FOV increases δ_{LPC} decreases, reaching a value of 0 beyond the physical boundary of the cloud. Rather than plotting δ_{LPC} as a function of range we can instead plot it as a function of optical depth τ for a fixed FOV, as in Figure 3.7b.

Depolarization as a function of FOV has been used by many groups to retrieve both particle size, optical depth, and particle phase. Early multiple scattering work used depolarization as

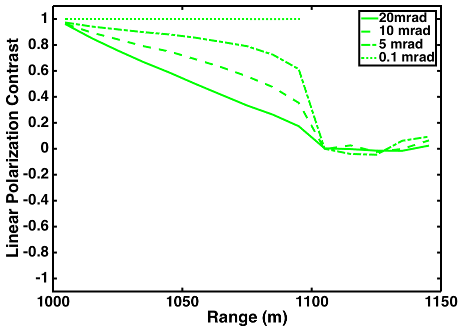

(a) Linear polarization contrast for clouds with size parameter $x = 0.74$ with $\tau_{\text{total}} = 3$ for different FOVs.

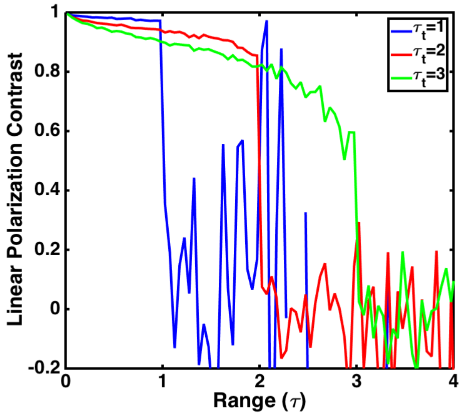

(b) Linear polarization contrast from clouds with size parameter $x = 0.74$ with a fixed field-of-view (5 mrad) and varying optical depth.

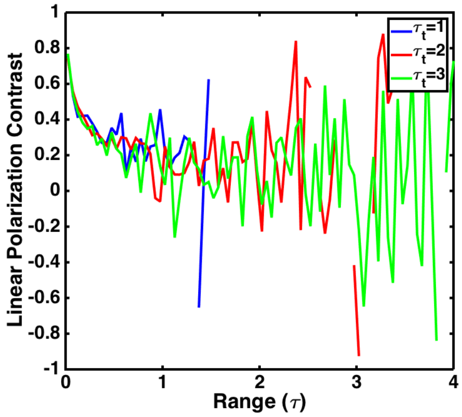

(c) Linear polarization contrast from clouds with size parameter $x = 8.43$ with a fixed field-of-view (5 mrad) and varying optical depth.

Figure 3.7: Different views of the linear polarization contrast

a measure of the amount of multiple scattering and tested theoretical results with the use of aperture stops, finding good empirical comparison to theory for small optical depths [37, 38, 39]. Vertical inhomogeneities in the cloud cause depolarization ratios to differ based on elevation angle of the lidar transmitter/receiver and depolarization ratios were seen to vary with time as the cloud composition changed [23]. The depolarization is also seen to depend on both droplet consistency and particle phase, with irregular-shaped ice crystals resulting in high depolarization values even for singly-scattered photons [24]. This is proposed for use as a method to determine differences between water- and ice-clouds and vertical phase-structure within a cloud from a satellite-based lidar system [25]. By looking at how the depolarization changes as a function of range, Kim et. al. were able to determine both liquid water content and effective particle radius without changing FOV [40, 41]. While there are proven retrieval methods for capturing microphysical properties from depolarization methods, by incorporating new methods these properties can be pinned down more accurately and various assumptions can be dropped. Depolarization measurements are plagued by the fact that many parameters (droplet size, optical density) contribute to changes in depolarization so finding an independent measure of one or both of these parameters would provide a stronger measure of microphysical properties.

3.4 Images

The azimuthal variation in the phase function shown in Figure 3.1 and Equation (2.2) suggests that there will be an azimuthal variation in the returned polarization patterns; the light in the two different polarization channels comes from different places in the cloud. These were first observed by Pal and Carswell [1] and attributed largely to second-order scattering [42, 18]. These patterns are shown in Figure 3.8 for the different polarization components. In all of these images, the initial polarization is horizontal. From the total signal and the co-polarized signal, it is apparent that the majority of the scattering is perpendicular to the initial polarization plane, as expected from the forms of the phase functions in Equation (2.2). The co-polarized signals show a two-fold symmetry around the polarization plane. The four-fold symmetry present in the cross-polarized signals arises from $R(\phi)$ in Equation (2.9) and $R(\psi)$ in Equation (2.11). These patterns have been analyzed semi-analytically [42, 43] and can be explained by the conservation of angular momentum of light [44]. This semi-analytical work has shown that there is information in these patterns regarding important microphysical properties of the cloud.

By comparing the co-polarized patterns returned from the small-particle cloud and from the large-particle cloud it is clear that there is some information on the particle size as the co-polarized signals are quite different (Figures 3.8c and 3.8d). Hielscher, Mourant, and Bigio exploit azimuthal variations in these patterns to learn about particle size, concentration, and anisotropy present in biological cell suspensions [45]. More recently, Griaznov et. al. developed a model with experimental predictions and tested it using a cross-shaped mask to isolate the contributions at different azimuthal angles[43]. Part of the problem with these azimuthal measurements is the difficulty in experimentally recording these patterns as a function of range into a cloud. Most measurements made so far involve very wide range-bins that typically include an entire cloud depth and so influences due to variations in particle size and concentration are integrated over and difficult to separate. Gated intensified charge coupled devices (ICCDs) have allowed for exactly this type of analysis [46].

In order to understand how the azimuthal patterns will evolve as a function of range through the cloud it helps to first investigate the azimuthal patterns due solely to second-order scattering. Figure 3.9 shows only the contributions from double-scattered photons. These patterns are identical to those created using semi-analytic methods [42]. Also shown are Pal and Carswell experimental images in Figures 3.9e and 3.9f showing excellent agreement with the double-scattered Monte Carlo results. The scattering from small particles shows a large difference between the full patterns and the second-order patterns which is because of contributions from higher scattering orders. The large particle full patterns on the other hand are quite similar to the second order patterns (compare Figure 3.8f and 3.9d). The phase function for the large particles is heavily peaked in the forward direction meaning that photons leave the cloud after fewer interactions than they do in the small-particle case. This means that optical depth does not always track well with the number of

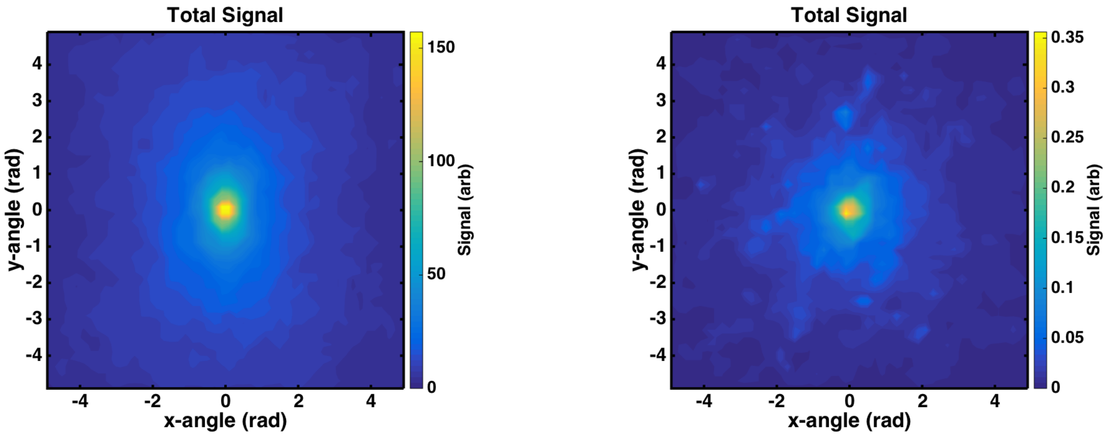

(a) Size parameter $x = 0.74$, $\tau_{\text{total}} = 3$ (b) Size parameter $x = 8.43$, $\tau_{\text{total}} = 3$

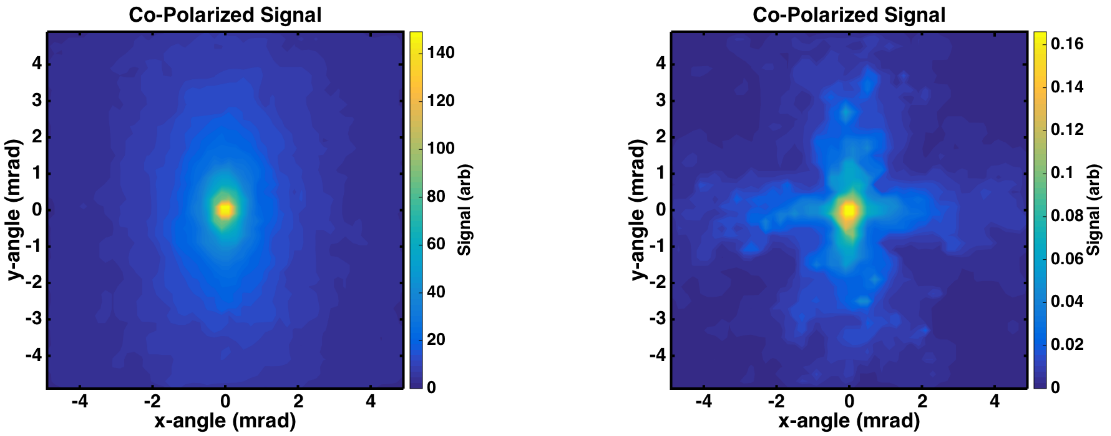

(c) Size parameter $x = 0.74$, $\tau_{\text{total}} = 3$ (d) Size parameter $x = 8.43$, $\tau_{\text{total}} = 3$

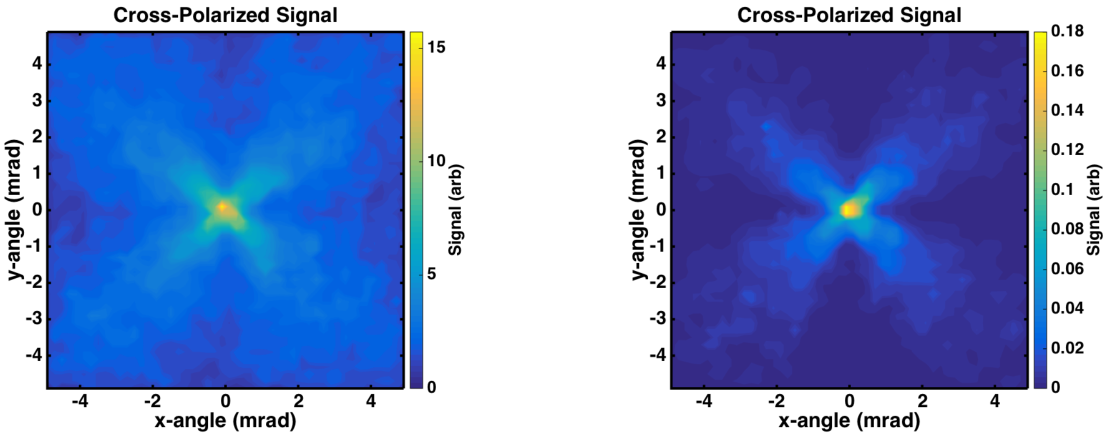

(e) Size parameter $x = 0.74$, $\tau_{\text{total}} = 3$ (f) Size parameter $x = 8.43$, $\tau_{\text{total}} = 3$

Figure 3.8: Images of the received signal as a function of received angle (which then translates into spatial position on a detector)

scattering events, as a simple picture might suggest.

The azimuthal dependence of the co- and cross-polarized signals is shown in Figure 3.10a. Semi-analytic methods to interpret doubly-scattered photons suggest that the azimuthal dependence of the cross-polarized returns should follow a $1 - \cos(4\phi)$ dependence [42]. This suggests that these signals can be fit to an equation of the form

$$I(\phi) = A + B\cos(4\phi) \tag{3.3}$$

where $A > 0$ and $B < 0$. The ratio between minima and maxima can then be defined as

$$R = \frac{I_{\text{min}}}{I_{\text{max}}} = \frac{A + B}{A - B} \tag{3.4}$$

The ratio for double-scattered photons should be exactly zero according to Rakovic and Kattawar [42]. As can be seen in Figure 3.10b the ratio for double-scattered photons is nearly zero while the contrast for all photons is nearly 1/2. Higher order scattering will blur the strong azimuthal patterns as seen when comparing Figure 3.9c with Figure 3.8e. Roy et. al. used this contrast to correlate the azimuthal contrast of the cross-polarized channel to the optical depth [46]. The change in contrast comes about through multiple scattering so perhaps a better way to analyze it is to correlate the contrast with number of scattering events.

Rather than take the contribution of all photons or only double-scattered photons as in Figure 3.10, it is possible to sort the returned photons into range-bins and thereby fit the azimuthal dependence as a function of range. Results from these fits are shown in Figures 3.11a for small particles. As the range into the cloud increases the ratio increases from near-zero up to a value of around 0.8. The ratio from Equation (3.4) is also calculated for double-, triple- and quadruple-scattered photons and these are plotted as broken blue lines. Also calculated are the average number of multiple-scattering events (so excluding single-scattered events) as a function of range and shown in Figures 3.11b. Note that for the large particles the average number of scattering events does not rise above 3 until past the edge of the cloud whereas for small particles the average number of scattering events increases continually through the cloud. This is again because of

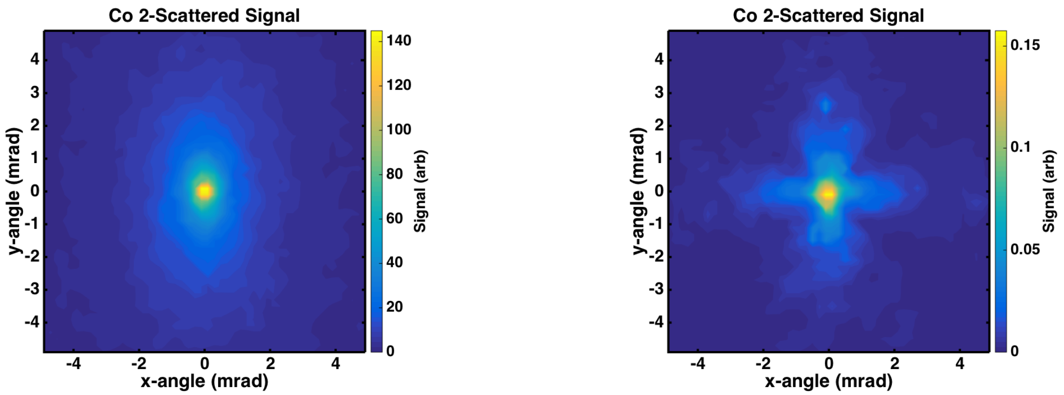

(a) Size parameter $x = 0.74$, $\tau_{\text{total}} = 3$ (b) Size parameter $x = 8.43$, $\tau_{\text{total}} = 3$

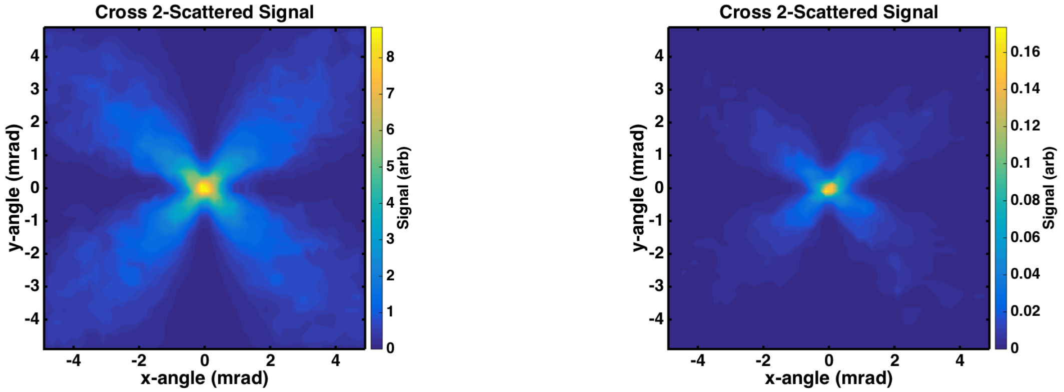

(c) Size parameter $x = 0.74$, $\tau_{\text{total}} = 3$ (d) Size parameter $x = 8.43$, $\tau_{\text{total}} = 3$

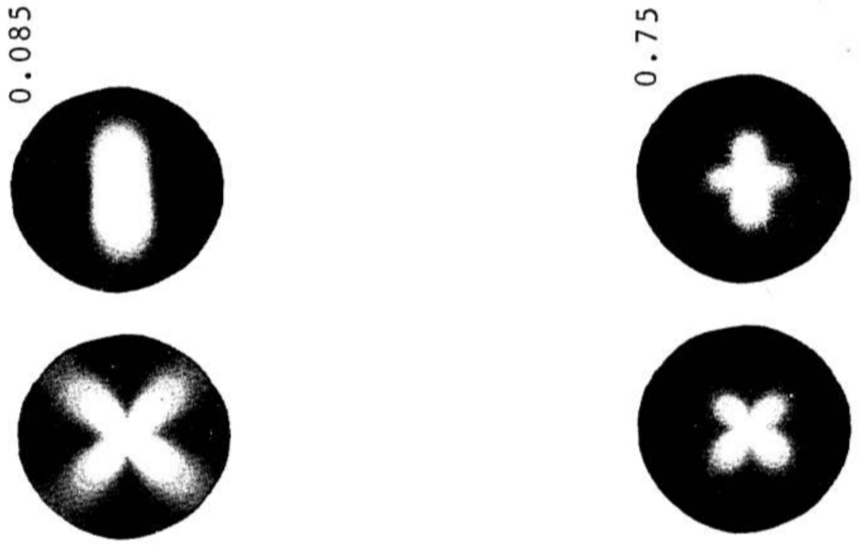

(e) Observed pattern for size parameter $x = 0.84$ [1] (f) Observed pattern for size parameter $x = 7.4$ [1]

Figure 3.9: Images of the received signal from double-scattered photons as a function of received angle (which then translates into spatial position on a detector). Also shown are observed patterns from [1] for similar size parameters.

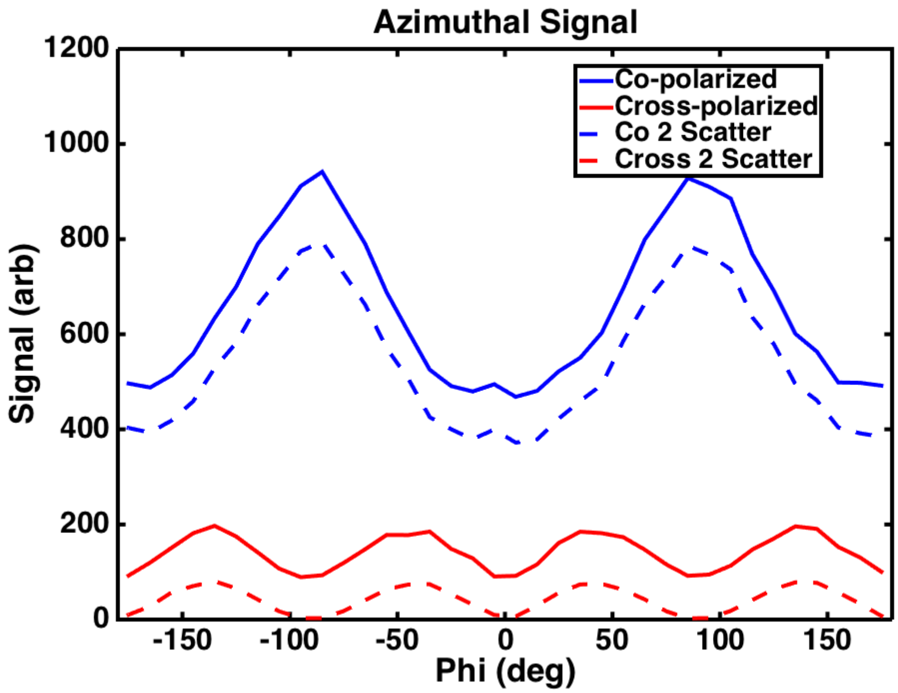

(a) Total and double-scattered azimuthal dependence for co- and cross-polarized signals for size parameter $x = 0.74$ with $\tau_{\text{total}} = 3$

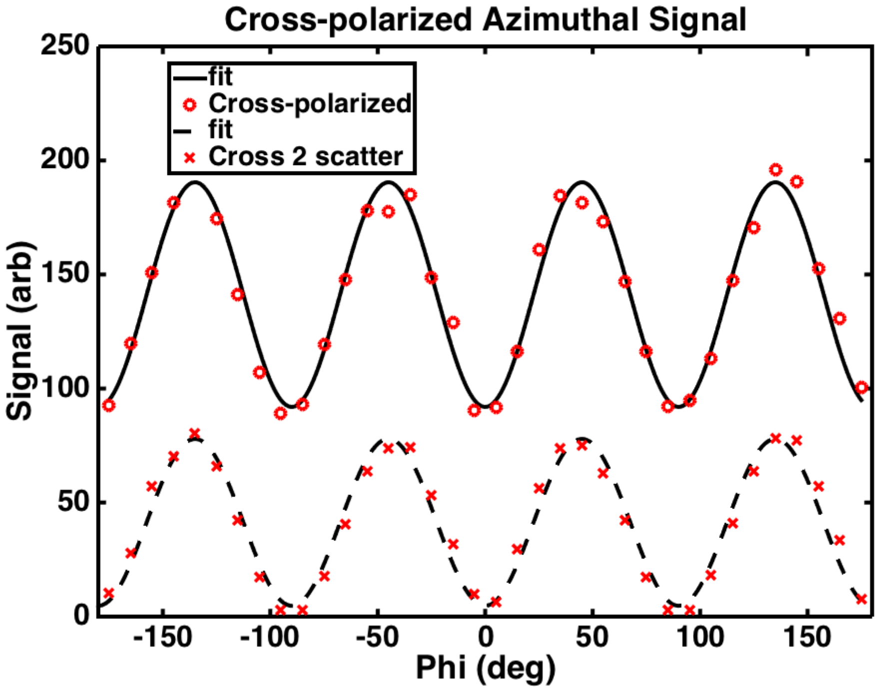

(b) Fits to total and double-scattered azimuthal dependence for cross-polarized signals for size parameter $x = 0.74$ with $\tau_{\text{total}} = 3$

Figure 3.10: Azimuthal dependence of returned photon from small-particle clouds

the highly-forward-peaked nature of the phase function for scattering from large particles. The azimuthal contrast ratio compares very well to the average multiple-scattering number. In the small-particle case the average number of scattering events reaches 3 at around 1060 m, which is where the contrast ratio reaches the triple-scattered line. Differentiating the number of scattering events above that is difficult with the statistics so far present because of the nearness of the triple- and quadruple-scattered contrast ratios. Likewise for the large-particle case, the ratio and the average scattering number track very well as neither extends beyond three through the whole cloud (again blurred somewhat due to low statistics).

This connection between number of scattering events and azimuthal contrast can be used also to measure the optical depth of the medium. If instead of plotting the azimuthal contrast as a function of distance we instead plot it as a function of optical depth then for clouds of three different optical densities, the curves collapse onto one another, as shown in Figure 3.11c. This means that by measuring the azimuthal contrast of the cross-polarized signal we have a good measure of the optical depth of the cloud. Note that this will change for different particle sizes because of the propensity for large particles to primarily scatter in the forward direction.

Given the difference in co-polarized images for scattering from particles with different size parameters (Figures 3.8c and 3.8d) we can fit the co-polarized azimuthal contrast to a form

$$I(\phi) = A + B\cos(2\phi) + C\cos(4\phi) \tag{3.5}$$

Azimuthal contrast and fits to this equation for different particle sizes are shown in Figure 3.12. We can then define a contrast which measures the intensity difference in two- and four-fold patterns

$$R = \frac{C+B}{C-B} \tag{3.6}$$

This ratio is shown in Figure 3.12c and shows a clear relation to particle size. Whether this extends over a wider range of sizes is yet to be investigated although this method has promise for providing an additional measure of particle size independent from measures of optical density.

The work presented here is a start towards a retrieval method for capturing real cloud properties from a lidar measurement, and serves more as a measuring framework to be tested with

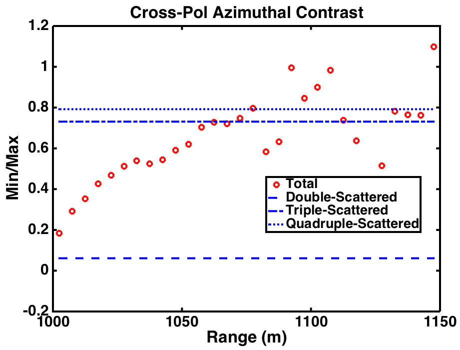

(a) Cross-polarized azimuthal contrast ratio as a function of range for scattering from clouds with size parameter $x = 0.74$. Shown also are fit values for exact scattering orders.

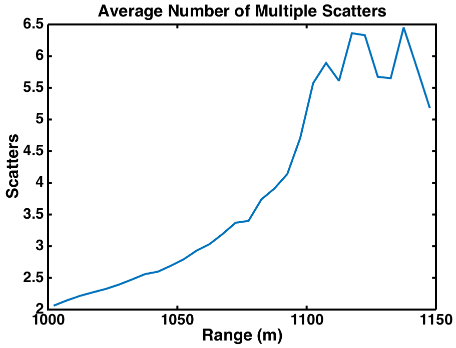

(b) Average number of multiple scattering events (excluding single-scattered photons) as a function of range for scattering from clouds with size parameter $x = 0.74$.

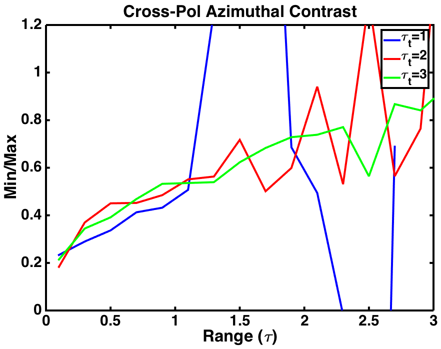

(c) Cross-polarized azimuthal contrast ratio for three different cloud densities plotted as a function of optical depth for clouds with size parameter $x = 0.74$.

Figure 3.11: Cross-polarized azimuthal contrast and its relation to number of scattering events and optical depth

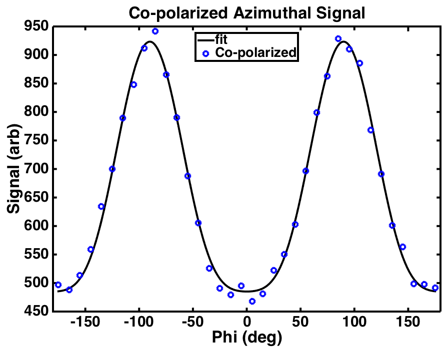

(a) Co-polarized azimuthal contrast ratio for depth-integrated scattering from clouds with size parameter $x = 0.74$. Shown also is the fit to Equation (3.5).

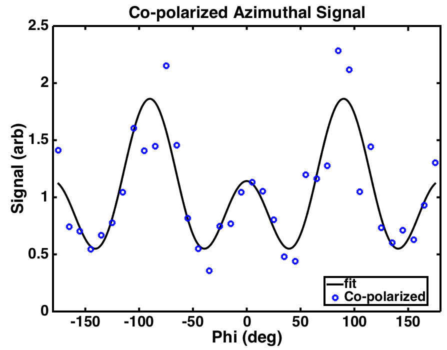

(b) Co-polarized azimuthal contrast ratio for depth-integrated scattering from clouds with size parameter $x = 8.43$. Shown also is the fit to Equation (3.5).

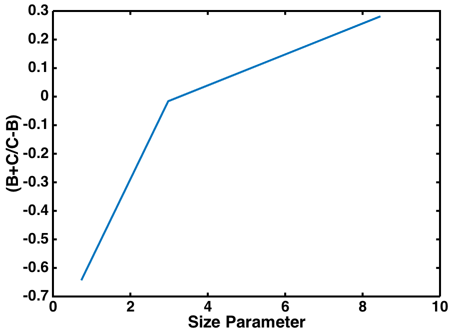

(c) Co-polarized contrast ratio is related to particle size.

Figure 3.12: Co-polarized azimuthal contrast and its relation to particle size.

further theoretical and experimental work.

Chapter 4

Moving Forward

It has been known for a long time that Monte Carlo simulations can aid in the interpretation and design of lidar systems [3]. In this thesis a Monte Carlo program has been demonstrated that brings together techniques from traditional lidar methods and studies of biological materials with the goal of studying optically dense media.

4.1 Towards Better Monte Carlo Simulations

The simulations presented in this thesis are simply a starting point in the Monte Carlo technique. In order to turn these programs into something with strong predictive power it will be necessary to more accurately model real-world conditions.

One adjustment that can be easily made is to adjust the geometry of the lidar problem. One instance where this would be useful is in defining the laser beam divergence. Real lasers are not infinitesimally thin as in the simulations presented here, and this will affect the signal returning from various FOVs especially with regards to single/multiple scattering ratio. For example, a finite laser beamwidth means that some single-scattered photons will arrive at a finite observed angle. This will have the effect of slightly blurring the images presented here.

The clouds used in this work are vastly different from real clouds in a few ways. The main difference is that the water droplets used here are too small for real clouds, they are actually representative of haze. Real clouds have particle distributions (they are not monodisperse) with a mean radius of around 10 μm which is much larger than the sizes used here. The rejection method of sampling the two-dimensional phase function becomes increasingly inefficient as the particle size gets larger because the phase function becomes more and more forward peaked. Finding a different method of sampling the phase function would allow for larger particles to be studied without a massive decrease in efficiency. Perhaps this efficiency hit is worth the increase in realism.

Mentioned above is that real clouds are not monodisperse and they also contain variations in density and phase. Determining the difference between ice-clouds and water-clouds is an important problem in remote sensing that could benefit from lidar penetration into clouds. Integrating a phase function for various-shaped ice-crystals into a Monte Carlo code would add to the predictive power.

Many current lidar systems measure depolarization at different fields-of-view to determine information about cloud particle size and density. The addition of images as described in this thesis would add to these measurements and provide independent measures of particle size and density. With the additional information, it is also possible that quantities such as index of refraction or droplet asphericity could be extracted as well, although that has not yet been investigated. There is promise that the images may contain valuable information that is complimentary to current lidar studies but more work has to be done on that front.

Finally, combining the results of a Monte Carlo program with a full Stokes Vector Lidar Equation would aid in the interpretation of signal strengths [47]. To do this would require turning the “Signal (arb)” axes presented in most graphs above into something more akin to a cross-section or signal-strength-per-N-photons.

Putting this all together would transform the Monte Carlo program into a much more powerful tool that could be coupled with an experimental program to investigate multiple scattering in real world systems.

4.2 Toward a MFOV Lidar System

Experimental verification of the work presented in this thesis would strengthen the code as well as provide avenues for future research. Toward this end a few ideas are presented here for designing a lidar system for measuring multiple scattering.

Many of the results presented are highly dependent on chosen parameters such as cloud distance, cloud depth, particle density, particle size, etc. When designing a lidar system the range of FOVs necessary to observe multiple scattering will be highly dependent on all of these so utilizing a Monte Carlo code will allow for predictions to be made and tested. Veselovskii et. al. show that in order to maximize information content in MFOV measurements, 5-6 different FOVs are necessary though the exact FOVs depend on experimental factors [36].

Some general adjustments that must be made in order to measure the azimuthal signals analyzed above will be discussed further. One method of capturing images is to use a charge-couple device (CCD) camera. Traditional CCD cameras do not have the time-sensitivity that would allow for range-resolved measurements, although as seen in Figure 3.8 there is still information to be had in these types of measurements. Far more can be learned however with range-resolved measurements. A recent advance that would allow for this is the use of gated intensified CCD (ICCD) cameras as in work by Roy et al. [46]. ICCD cameras have the capability to be gated in time, allowing for the measurement of very narrow (ns) time slices. For each laser shot, only a single time slice could be measured and many laser pulses would have to be integrated to produce a final image for that particular time slice. Measurement in this way of a full depth profile could be time consuming depending on the signal levels returned from the cloud.

Another method that would allow for measurement of azimuthal signal would be the use of a spatial mask placed at a focal plane of the receiver, as shown for the cross polarized signal in Figure 4.1. Light that passes through the mask would all be focused onto a single-element detector such as a photomultiplier tube (PMT) or a photodiode. This spatial mask could be designed to isolate different parts of the expected pattern, allowing for measurements like the contrast presented in Figures 3.11 and 3.12 to be made experimentally. By rotating in different spatial masks into co- and cross-polarized channels and relying on symmetries present in the images, determination of azimuthal contrast would be possible. The contrast between the total signal shown making it through the mask in Figure 4.1a and that making it through in Figure 4.1b is analogous to the azimuthal contrast presented in Figure 3.10 and 3.11. This method allows for an imperfect measure of the contrast which will in turn provide information on the optical depth of the medium.

A similar mask can be created for measuring the co-polar variations, although designing the mask is somewhat trickier due to the subtler differences in scattering profiles between particles of different sizes, as shown in Figure 4.2. The larger particles lead to a much stronger peak along the horizontal axis ($\phi = 0°, 180°$) compared to smaller particles. With more realistic (larger) droplet sizes these differences could change significantly.

The phase function for 10 micron water droplet, which is more in line with real water clouds, is shown in Figure 4.3. There are many lobes at 0, 90, 180, 270, and 360 degrees which will contribute to similar patterns as those shown in Figure 4.2, although whether that will be enough to differentiate various sized particles needs to be investigated.

Monte Carlo codes for radiative transfer have been shown to be useful for simulating experimental conditions. In this thesis it is demonstrated that multiply scattered light carries information about the medium that is manifested in changes in polarization and received direction. It is then possible to extract this information in an experimental situation to learn about the properties of the scattering medium. With a Monte Carlo code, various experimental parameters and retrieval algorithms can be adjusted and tested in a short amount of time. Continuing work in this vein would increase our ability to remotely monitor optically dense media.

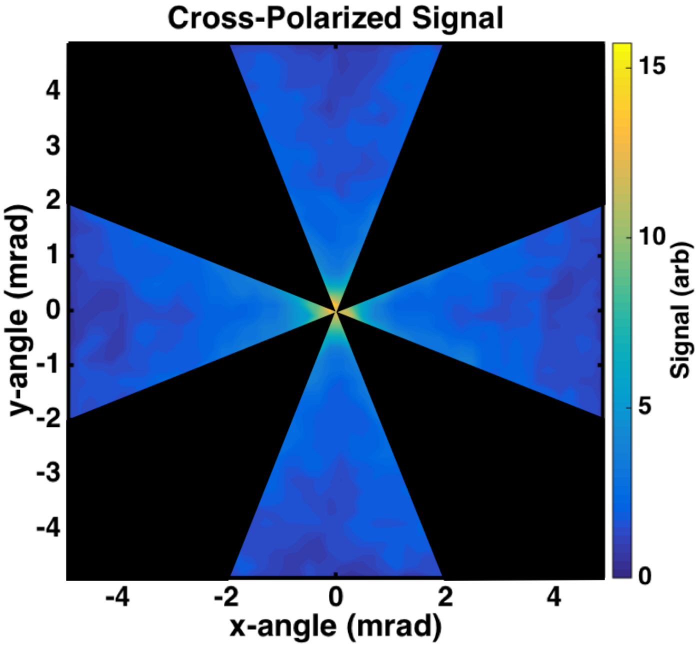

(a) Spatial mask that captures the minimum of the azimuthal variation of the cross-polarized signal

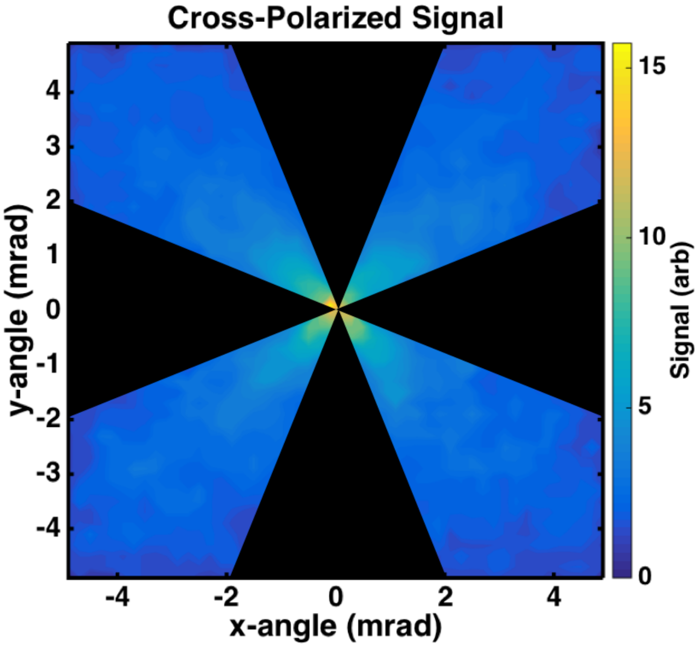

(b) Spatial mask that captures the maximum of the azimuthal variation of the cross-polarized signal

Figure 4.1: Possible spatial masks for cross-polarized images

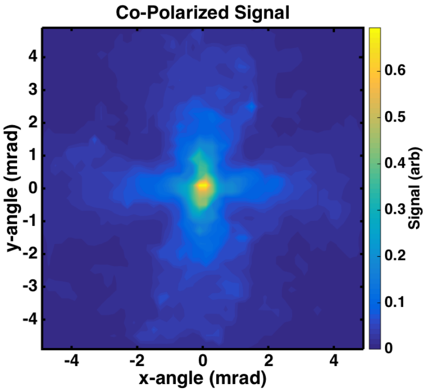

(a) $x = 8.43$

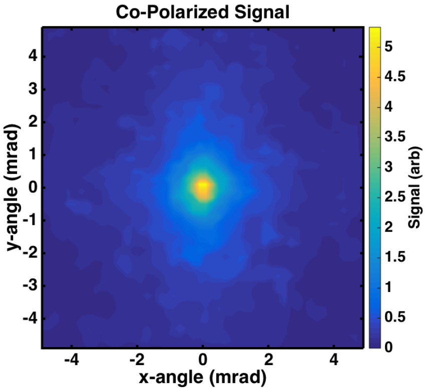

(b) $x = 2.98$

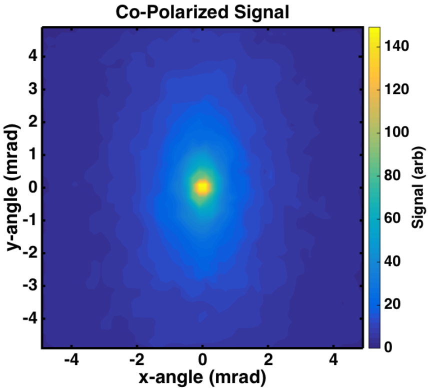

(c) $x = 0.744$

Figure 4.2: Spatial images for the co-polarized depth-integrated signal coming from clouds made up of particles with different size parameters and the same total optical depth $\tau_{\text{total}} = 3$.

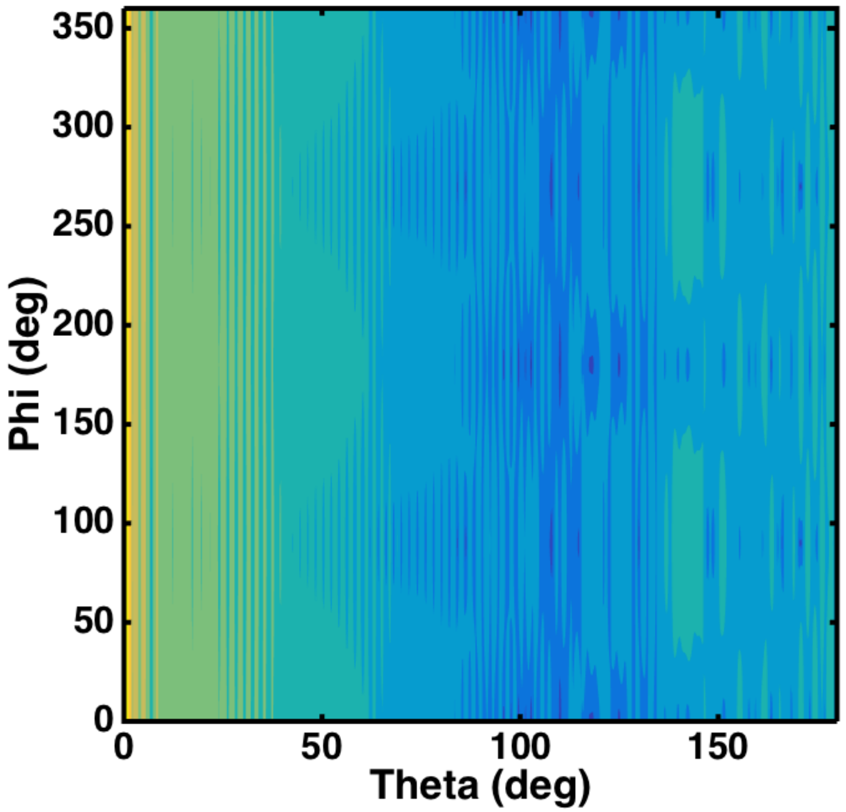

Figure 4.3: Phase function for 10 micron radius water droplets with 633 nm light. Theta and phi are the scattering polar and azimuthal angles, respectively. The phase function is colored by the log of its value with yellow being maximum and blue being minimum.

Bibliography

[1] S. R. Pal and A. I. Carswell, "Polarization anisotropy in lidar multiple scattering from clouds," Applied optics, vol. 25, p. 4228, Dec. 1986.

[2] S. E. Mitchell and J. P. Thayer, "Ranging through Shallow Semitransparent Media with Polarization Lidar," Journal of Atmospheric and Oceanic Technology, vol. 31, pp. 681–697, Mar. 2014.

[3] L. R. Bissonnette, "Lidar and Multiple Scattering," in Lidar: Range Resolved Optical Remote Sensing of the Atmosphere (C. Weitkamp, ed.), pp. 43–103, Springer Science+Business Media Inc, 2005.

[4] J. E. Milton, R. C. Anderson, and E. V. Browell, "Lidar Reflectance of Fair-Weather Cumulus Clouds at 0 . 903 μ," Applied Optics, vol. 11, no. 3, p. 697, 1971.

[5] S. R. Pal, J. S. Ryan, and A. I. Carswell, "Cloud reflectance with Laser Beam Illumination," Applied optics, vol. 17, no. 15, p. 2257, 1978.

[6] N. Metropolis and S. Ulam, "The Monte Carlo Method," Journal of the American Statistical Association, vol. 44, pp. 335–341, Sept. 1949.

[7] G. W. Kattawar and G. N. Plass, "Radiance and polarization of multiple scattered light from haze and clouds.," Applied optics, vol. 7, pp. 1519–27, Aug. 1968.

[8] G. W. Kattawar and G. N. Plass, "Influence of particle size distribution on reflected and transmitted light from clouds.," Applied optics, vol. 7, no. 5, pp. 869–878, 1968.

[9] G. N. Plass and G. W. Kattawar, "Monte carlo calculations of light scattering from clouds.," Applied optics, vol. 7, pp. 415–9, Mar. 1968.

[10] G. N. Plass and G. W. Kattawar, "Calculations of Reflected and Transmitted Radiance for Earth's Atmosphere.," Applied optics, vol. 7, no. 6, pp. 1129–1135, 1968.

[11] G. N. Plass and G. W. Kattawar, "Radiant intensity of light scattered from clouds.," Applied optics, vol. 7, no. 4, pp. 699–704, 1968.

[12] G. N. Plass and G. W. Kattawar, "Reflection of light pulses from clouds.," Applied optics, vol. 10, pp. 2304–10, Oct. 1971.

[13] K. Kunkel and J. Weinman, "Monte Carlo Analysis of Multiply Scattered Lidar Returns," Journal of the Atmospheric Sciences, vol. 33, p. 1772, 1976.

[14] L. R. Poole, D. D. Venable, and J. W. Campbell, “Semianalytic Monte Carlo radiative transfer model for oceanographic lidar systems.,” Applied optics, vol. 20, pp. 3653–6, Oct. 1981.

[15] L. R. Poole, “Computed laser backscattering from turbid liquids: comparison with laboratory results.,” Applied optics, vol. 21, pp. 2262–4, June 1982.

[16] C. Platt, “Remote sounding of high clouds. III: Monte Carlo calculations of multiple-scattered lidar returns,” Journal of the atmospheric sciences, vol. 38, 1981.

[17] P. Bruscaglioni, A. Ismaelli, and G. Zaccanti, “Monte-Carlo calculations of LIDAR returns : Procedure and results,” Applied Physics B, vol. 329, pp. 325–329, 1995.

[18] M. J. Rakovic, G. W. Kattawar, M. B. Mehrubeolu, B. D. Cameron, L. V. Wang, S. Rastegar, and G. L. Coté, “Light backscattering polarization patterns from turbid media: theory and experiment.,” Applied optics, vol. 38, pp. 3399–408, May 1999.

[19] S. Bartel and A. H. Hielscher, “Monte Carlo Simulations of the Diffuse Backscattering Mueller Matrix for Highly Scattering Media,” Applied Optics, vol. 39, p. 1580, Apr. 2000.

[20] J. C. Ramella-Roman, S. A. Prahl, and S. L. Jacques, “Three Monte Carlo programs of polarized light transport into scattering media: part I,” Optics Express, vol. 13, no. 12, pp. 148–163, 2005.

[21] C. F. Bohren and D. R. Huffman, Absorption and scattering of light by small particles, vol. 1. John Wiley & Sons, 1983.

[22] S. A. Prahl, “http://omlc.org/software/mie/.”

[23] K. Sassen and R. Petrilla, “Lidar depolarization from multiple scattering in marine stratus clouds,” Applied optics, vol. 25, no. 9, 1986.

[24] K. Sassen, H. Zhao, and B. K. Yu, “Backscatter laser depolarization studies of simulated stratospheric aerosols: crystallized sulfuric acid droplets.,” Applied optics, vol. 28, pp. 3024–9, Aug. 1989.

[25] Y.-x. Hu, D. Winker, P. Yang, B. Baum, and L. Poole, “Identification of cloud phase from PICASSO-CENA lidar depolarization : a multiple scattering sensitivity study,” Journal of Quantitative Spectroscopy and Radiative Transfer, vol. 70, pp. 569–579, 2001.

[26] S. R. Pal and a. I. Carswell, “Multiple scattering in atmospheric clouds: lidar observations.,” Applied optics, vol. 15, no. 8, pp. 1990–1995, 1976.

[27] A. V. Starkov, M. Noormohammadian, and U. G. Oppel, “A stochastic model and a variance-reduction Monte-Carlo method for the calculation of light transport,” Applied Physics B Laser and Optics, vol. 60, pp. 335–340, Apr. 1995.

[28] D. M. Winker, L. R. Poole, and A. S. Division, “Monte-Carlo calculations of cloud returns for ground-based and space-based LIDARS,” Applied Physics B, vol. 344, pp. 341–344, 1995.

[29] L. R. Bissonnette, P. Bruscaglioni, A. Ismaelli, G. Zaccanti, A. Cohen, Y. Benayahu, M. Kleiman, S. Egert, C. Flesia, P. Schwendimann, a. V. Starkov, M. Noormohammadian, U. G. Oppel, D. M. Winker, E. P. Zege, I. L. Katsev, and I. N. Polonsky, “LIDAR multiple scattering from clouds,” Applied Physics B Laser and Optics, vol. 60, pp. 355–362, Apr. 1995.

[30] L. R. Bissonnette, “Multiple-scattering lidar equation.,” Applied optics, vol. 35, pp. 6449–65, Nov. 1996.

[31] L. R. Bissonnette and D. Hutt, “Multiple scattering lidar,” Applied optics, vol. 29, no. 34, pp. 5045–5046, 1990.

[32] D. L. Hutt, L. R. Bissonnette, and L. Durand, “Multiple field of view lidar returns from atmospheric aerosols.,” Applied optics, vol. 33, pp. 2338–48, Apr. 1994.

[33] G. Roy, L. R. Bissonnette, C. Bastille, and G. Vallée, “Retrieval of droplet-size density distribution from multiple-field-of-view cross-polarized lidar signals: theory and experimental validation,” Applied optics, vol. 38, no. 24, 1999.

[34] G. Roy and N. Roy, “Standoff determination of the particle size and concentration of small optical depth clouds based on double scattering measurements: concept and experimental validation with bioaerosols,” Applied Optics, vol. 47, p. 1336, Mar. 2008.

[35] L. R. Bissonnette, G. Roy, L. Poutier, S. G. Cober, and G. a. Isaac, “Multiple-scattering lidar retrieval method: tests on Monte Carlo simulations and comparisons with in situ measurements.,” Applied optics, vol. 41, pp. 6307–24, Oct. 2002.

[36] I. Veselovskii, M. Korenskii, V. Griaznov, D. N. Whiteman, M. McGill, G. Roy, and L. R. Bissonnette, “Information content of data measured with a multiple-field-of-view lidar,” Applied Optics, vol. 45, no. 26, p. 6839, 2006.

[37] S. R. Pal and a. I. Carswell, “Polarization properties of lidar backscattering from clouds.,” Applied optics, vol. 12, no. 7, pp. 1530–1535, 1973.

[38] J. S. Ryan and A. I. Carswell, “Laser beam broadening and depolarization in dense fogs,” Journal of the Optical Society of America, vol. 68, p. 900, July 1978.

[39] J. S. Ryan, S. R. Pal, and A. I. Carswell, “Laser backscattering from dense water-droplet clouds,” Journal of the Optical Society of America, vol. 69, no. 1, pp. 60–67, 1979.

[40] D. Kim, H. D. Cheong, Y. Kim, S. Volkov, and J. Lee, “Optical depth and multiple scattering depolarization in liquid clouds,” Optical review, vol. 17, no. 6, pp. 507–512, 2010.

[41] D. Kim and J. Lee, “Measuring cloud droplet effective radius and liquid water content using changes in degree of linear polarization along cloud depth.,” Optics letters, vol. 39, pp. 3378–81, June 2014.

[42] M. J. Rakovic and G. W. Kattawar, “Theoretical analysis of polarization patterns from incoherent backscattering of light,” Applied Optics, vol. 37, no. 15, 1998.

[43] V. Griaznov, I. Veselovskii, P. Di Girolamo, M. Korenskii, and D. Summa, “Spatial distribution of doubly scattered polarized laser radiation in the focal plane of a lidar receiver.,” Applied optics, vol. 46, no. 27, pp. 6821–6830, 2007.

[44] C. Schwartz and A. Dogariu, “Backscattered polarization patterns determined by conservation of angular momentum,” Journal of the Optical Society of America A, vol. 25, no. 2, p. 431, 2008.

[45] A. H. Hielscher, J. R. Mourant, and I. J. Bigio, “Influence of particle size and concentration on the diffuse backscattering of polarized light from tissue phantoms and biological cell suspensions,” Applied Optics, vol. 36, p. 125, Jan. 1997.

[46] N. Roy, G. Roy, L. R. Bissonnette, and J.-R. Simard, “Measurement of the azimuthal dependence of cross-polarized lidar returns and its relation to optical depth.,” Applied optics, vol. 43, pp. 2777–85, May 2004.

[47] M. Hayman and J. P. Thayer, “General description of polarization in lidar using Stokes vectors and polar decomposition of Mueller matrices.,” Journal of the Optical Society of America. A, Optics, image science, and vision, vol. 29, pp. 400–9, Apr. 2012.